

Ab Initio Characterization of $C_2H_4N_2$ Isomers: Structures, electronic energies, spectroscopic parameters and formation pathways

Oko Emmanuel Godwin,¹ Natalia Inostroza,¹ Diego Mardones,² Luca Bizzocchi,³ Edgar Mendoza,⁴ María Luisa Senent,⁵ and Miguel Carvajal⁶

¹⁾Universidad Autónoma de Chile, Facultad de Ingeniería, Instituto de Ciencias Aplicadas, Núcleo de Astroquímica & Astrofísica, Av. Pedro de Valdivia 425, Providencia, Santiago, Chile

²⁾Universidad de Chile, Facultad de Ciencias Físicas y Matemáticas, Departamento de Astronomía, Camino el Observatorio 1515, Las Condes, Santiago, Chile

³⁾Dipartimento di Chimica “Giacomo Ciamician”, via P. Gobetti 85, Università di Bologna, Bologna, Italy

⁴⁾Dept. Ciencias Integradas, Facultad de Ciencias Experimentales, Centro de Estudios Avanzados en Física, Matemática y Computación, Unidad Asociada GIFMAN, CSIC-UHU, Universidad de Huelva, Spain

⁵⁾Departamento de Química y Física Teóricas, Instituto de Estructura de la Materia, IEM-CSIC, 28006 Madrid, Spain; Unidad Asociada GIFMAN, CSIC-UHU, Universidad de Huelva, 21071 Huelva, Spain

⁶⁾Dept. Ciencias Integradas, Facultad de Ciencias Experimentales, Centro de Estudios Avanzados en Física, Matemática y Computación, Unidad Asociada GIFMAN, CSIC-UHU, Universidad de Huelva, Spain

Instituto Universitario Carlos I de Física teórica y computacional, Universidad de Granada, Spain

(*Electronic mail: natalia.inostrozapino@gmail.com)

(Dated: January 13, 2026)

This work presents a comprehensive theoretical investigation of key isomers of $C_2H_4N_2$ using state-of-the-art quantum chemical methods. The objective is to characterize their molecular structures, spectroscopic constants, and electronic energies, and elucidate plausible formation and destruction pathways, providing data critical for astrochemical and atmospheric detection. High-accuracy *ab initio* methods were employed, notably CCSD(T)-F12/cc-pVTZ-F12 for optimized geometries. Additional calculations were performed at the CCSD(T)/aug-cc-pVTZ, CCSD(T)/cc-pVTZ, MP2/aug-cc-pVTZ, and CIS levels. Intrinsic reaction coordinate (IRC) calculations were performed at the B3LYP / 6-31G(d, p) level to explore reaction pathways. The ZPE-corrections were determined for all of the isomers considered. Six low-energy $C_2H_4N_2$ isomers were identified, all within 1 eV of the global minimum. Among them, methylcyanamide (MCA) exhibits the lowest relative energy (~0.2 eV) and a significant electric dipole moment of 5.00 D, making it a strong candidate for detection in the gas phase environments. The rotational constants for MCA, computed at the level of CCSD(T)-F12/cc-pVTZ-F12, are $A_e = 34,932.44$ MHz, $B_e = 4,995.31$ MHz and $C_e = 4,520.30$ MHz. The V_3 torsional barrier was found to be 631.19 cm^{-1} . Centrifugal distortion constants were computed up to sextic order for all isomers. Formation pathways for MCA —such as $CH_3N + HCN \rightarrow CH_3NHCN$ — and related isomers were characterized. The combination of large dipole moments and distinct rotational signatures supports the detectability of methylcyanamide and related $C_2H_4N_2$ isomers via radioastronomy, IR and MW spectroscopy. Isomerization and reaction pathways involving radical neutral and neutral neutral processes were found to be key to their formation in the gas phase environments. These results offer a robust foundation for future observational and modeling efforts.

I. INTRODUCTION

In the atmosphere, N-bearing molecules such as amines ($R-NH_2$) and nitriles ($R-C\equiv N$) either in the gas phase or particle-phase find their ways into the atmosphere via sources such as industrial wastes, biomass burning, vehicle exhaust fumes, carbon capture and storage (CCS) technologies, agricultural waste, animal husbandry, etc.¹. Measurements indicate that the amount of amines in the Earth’s atmosphere has increased over the years enhancing aerosol formation and growth rates, aerosol hygroscopicity, and the activation of cloud condensation nuclei². It is now known that these sources cause amine emissions that lead to rich chemistry in the gas phase, which produces intermediates and conversion products converting amines to amides, imines and many other

products known to contribute substantially to global climate effects, global mortality rate, diminishing agricultural production, toxicity, etc.^{1,3}. Under this context, Nielsen, Herrmann, and Weller³ showed that reactions between OH radical and alkyl amine occur very quickly, with a rate coefficient $> 10^{11} cm^3 molecule^{-1} s^{-1}$. These reactions contribute to a major sink of alkylamines in the gas phase and typically they diminish within 6 hours in the atmosphere.

Reactive N-bearing species such as methylamidogen radical $CH_3N^{\cdot}H$ with $\cdot NO$ and others bring about the formation of intermediates or products responsible for the cascading effects of N-bearing species and/or the variation in observed abundances of N-bearing species compared to models^{4–6}.

Beyond Earth atmosphere, N-bearing species are important for astrophysical environments as they are very abundant

dant in the Taurus molecular cloud⁷. Thus, the study of such molecular species, reaction processes and the spectral characterization of N-bearing compounds plays an important role in understanding the formation processes of other prebiotic/biological molecules and learn about the physical conditions of the environments where they are formed, such as exoplanet atmosphere and the interstellar medium (ISM)^{8–12}. Hence the accurate investigation of their structures, spectroscopy, and formation pathways are prerequisites for successful research.

In the interstellar medium, most N-bearing compounds such as hydrogen cyanides (HCN), cyanamide (NH_2CN and its tautomeric form HNCNH) are believed to be precursors of purines, pyrimidines and nucleobases¹³. These types of compounds are very reactive due to the presence of the nucleophilic amine and the electrophilic nitrile groups. Most of the isomers of the general formula $\text{C}_2\text{H}_4\text{N}_2$ fall into this group (amines, nitriles or both).

Apart from the well known isomer aminoacetonitrile (AAN, $\text{NH}_2\text{CH}_2\text{CN}$) which has been studied extensively and observed in the interstellar medium (ISM)^{14,15}, not much is known about the isomer methylcyanamide (CH_3NHCN , MCA or C1 hereafter). MCA could be a possible intermediate species in the formation of other N or CN-bearing compounds. There is only a spectral measurement published by Bak and Svanholt¹⁶ although no many assignments are reported. From the spectral assignments, only the rotational constants B and C could be determined with 0.07 MHz accuracy and, therefore, the structure was assumed from other related molecules such as CH_3NHCl . Without a good description of the structural and spectroscopic parameters, identification is challenging¹⁷. In addition, the vibrational frequencies and spectroscopic constants of 1,2-diiminoethane (NHCHCHNH) was recently investigated as promising molecules for astronomical detection¹⁸. These species fall under the general formula $\text{C}_2\text{H}_4\text{N}_2$ as the only known investigated species.

Theoretical *ab initio* methods become highly pertinent to describe the rotational structure and the vibrational interactions of these molecules as their anharmonic effects are significantly contributing to the observed spectra. According to Nair *et al.*¹⁹, Inostroza and Senent²⁰, McCarthy and Lee²¹ these constants such as rotational constants, centrifugal distortion constants, dipole moments, etc. are crucial to achieve accurate structural description and, in extension, enable potential detection of these species in the gas phase environments²². Currently, there is dearth of information available for these species in the literature. In particular, MCA as an isomer of the family $\text{C}_2\text{H}_4\text{N}_2$ also exhibits large amplitude motions (LAMs) associated with their lowest vibrational mode¹⁶ and, as such, it is important to investigate MCA and the other isomers of this family providing parameters that best describe them. This could be the case of MCA, because it exhibits LAM motions (such as the NH inversion motion and the methyl rotation) which descriptions constitute a challenge¹⁶.

In this contribution, we aimed to carry out high-quality *ab initio* molecular structure calculations for all isomers in their singlet ground electronic state (${}^1\text{A}_1$) as well as electronic excitation energies for the six most stable isomers. We

investigated the potential energy surface of $\text{C}_2\text{H}_4\text{N}_2$ including several novel isomers and some conformers. All isomers reported in this work are new additions to the literature except for aminoacetonitrile (AAN) and diiminoethane, which are added to the current work for comparison. We computed spectroscopic constants and pathways of formation for some key isomers of low energy. We provide, and compare when available, spectroscopic parameters such as vibrational frequencies, rotational constants, centrifugal distortions constants, dipole moments, and new pathways of formation and destruction of the three low energy isomers of close identity.

This paper is organised as follows: Section I is the introduction of N-bearing species in the atmosphere and the ISM, narrowing down to the $\text{C}_2\text{H}_4\text{N}_2$ isomers, along with the aims and motivations for this study. The next section II covers the methods used. Our findings and discussion are presented in section III covering structural characterisations, electronic energies, spectroscopic parameters, reaction pathways, the implications of the studied molecules and their formation and destruction pathways in atmospheric and astrophysical contexts, and the last section IV is the conclusion.

II. COMPUTATIONAL METHODS

The electronic structure and energy calculations of the molecular species $\text{C}_2\text{H}_4\text{N}_2$ were carried out with the explicitly correlated coupled cluster theory with single and double substitutions and a perturbative correction for the connected triple excitations CCSD(T)-F12^{23,24} using Molpro 2015.1 version²⁵. Throughout this paper, all reported CCSD(T)-F12 energies correspond to the CCSD(T)-F12b.

The F12 approach accelerates basis-set convergence, providing near-CBS energies without requiring augmented F12 basis sets²⁶, thus explicitly correlated Dunning basis set²⁷ cc-pVTZ-F12 was employed in this work as it provides a more efficient, lower-cost option that still offers good accuracy for many ground-state calculations and designed for CCSD(T)-F12²⁸. Other levels of theory were also considered, taking into account the required accuracy and the available computational resources. All other theoretical calculations, i.e., MP2²⁹ and CCSD(T)³⁰, were performed using both Gaussian 09 and Gaussian 16 suites of programs Frisch *et al.*^{31,32} as well as Automaton³³, which was used to search for the local minima of isomers (and conformers) along the $\text{C}_2\text{H}_4\text{N}_2$ potential energy surface (PES). Vertical excitation calculations were conducted using single excitation configuration interaction (CIS)³⁴ to analyse the excitation energies of the first six (6) most stable isomers.

Vibrational analysis, including anharmonic correction terms, of the fundamental frequencies of the molecular species $\text{C}_2\text{H}_4\text{N}_2$ was performed at CCSD(T)/cc-pVTZ³⁵ and MP2/aug-cc-pVTZ levels of theory²⁹ for low-lying isomers. PES of the large amplitude motions of the methylcyanamide (MCA, CH_3NHCN) was characterised at MP2/aug-cc-PVTZ level of theory. Rotational constants and dipole moments (μ) of $\text{C}_2\text{H}_4\text{N}_2$ isomers (and conformers) were calculated at corresponding equilibrium geome-

tries with CCSD(T)-F12/cc-pVTZ-F12, CCSD(T)/cc-pVTZ and MP2/aug-cc-pVTZ methods.

Reactions leading to the formation and destruction of MCA and other close-lying isomers were investigated within the framework of the Intrinsic Reaction Coordinate (IRC)^{36–39} approach using the default settings in Gaussian 09 and Gaussian 16. B3LYP/6-31G(d,p) level of theory was used to compute the IRC pathways due to its good compromise between accuracy and computational cost⁴⁰. Single-point energy calculations of the transition states were performed with the high-level coupled cluster CCSD(T) and MP2 levels of theory using a large augmented correlation-consistent polarised valence triple-zeta aug-cc-pVTZ basis set⁴¹. The structures at the minima and transition states were investigated using vibrational analysis obtained by B3LYP using analytical second-order derivative along the path connecting the transition state to intermediate, reactants, and products³⁷.

III. RESULTS AND DISCUSSION

A. Electronic energies of C₂H₄N₂ family

In Fig. 1 structures of eighteen isomers of the chemical formula C₂H₄N₂ are presented with their equilibrium geometries, energies relative to the most stable isomer E_{rel} (cm⁻¹), zero-point vibrational energies ZPVE(cm⁻¹), relative energies corrected with ZPVE, E_{rel}^{+ZPVE} (cm⁻¹), and their dipole moments μ (D). All these quantities are calculated using the level of theory CCSD(T)-F12/cc-pVTZ-F12, except the zero-point vibrational energy corrections, which is obtained from the CCSD(T)/cc-pVTZ. In fact, the E_{rel}^{+ZPVE} presented in Fig. 1 are calculated using the following approximate approach which provides accurate corrections for the energies⁴²:

$$E_{\text{rel}}^{+ZPVE} = \Delta E^{\text{CCSD}(T)-F12} + \Delta E_{\text{ZPVE}}^{\text{CCSD}(T)}, \quad (1)$$

where the energies are computed at the higher-level explicitly correlated coupled-cluster CCSD(T)-F12/cc-pVTZ-F12, and the zero-point vibrational corrections are obtained from the CCSD(T)/cc-pVTZ level.

Some of the characteristic features of the compounds presented in Fig. 1 include structural and geometric isomerism. All these structures are singlet electronic ground states deduced from the molecular orbitals and the spin multiplicity. The point groups (P.G.) of these isomers are also given. The isomers in Fig. 1 are labeled as A_n and C_n (n=1, 2, 3, ...), when they are aminoacetonitrile derivatives and cyanomethylamine derivatives, respectively: aminoacetonitrile (AAN or A1), methylcyanamide (MCA or C1), methylcarbodiimide (C2), diiminoethane (A2), trans-diiminoethane (A3), methanimidoylformimidamide (C3), aminoethanimine (A4), 2-aminomethylidenaziridine (C4), 2H-azirine (C5), bent-1,2-diazabutadiene (C6), ethynediamine (A5), trans-ethenediazine (C7), cis-ethenediazine (C8), 3-Methyl-3H-diazirine (C9), trans-hydrazinylethyne (C10), hydrazonoethene (C11), linear-1,2-diazabutadiene(C12), and trans-hydrazinylethyne (C13).

The relative energy E_{rel} of the molecular species of C₂H₄N₂ at the CCSD(T)-F12/cc-pVTZ-F12 level of theory are given in Fig. 1. They are relevant to predict the potentially observable isomers under different sources. Here it can be noted that the isomer AAN (also named A1), of which the spectrum has been recorded⁴³ is in fact the only isomer from C₂H₄N₂ family that has been observed in the ISM¹⁵. The next isomer in energy, MCA or C1, is only at 0.27 eV from A1 isomer. According to the minimum energy principle, the most stable isomer is usually the most abundant one^{44,45}. Thus, in line with our calculations, we expect that MCA (or C1), the second most stable, should also be observed in the ISM. In addition, we also present other isomers, A_n and C_n with lower E_{rel} . The relative energies (E_{rel}) of six lowest-energy isomers sorted based on increasing order: C2 (0.43 eV) < A2 (0.54 eV) < A3 (0.61 eV) < C3 (0.81 eV), placing all four structures within the 0.4–0.8 eV energy range above the global minimum.

From the family of C₂H₄N₂, we can distinguish, among all the molecular structures shown in Fig. 1, the pairs A2 and A3, C7 and C8 as conformers, while C6 is stable but the matching pair C12 is a transition state, C10 is stable whereas the matching pair C13 is a transition state. The energy gaps between the pairs of conformers C6 and C12 and C10 and C13 are large enough and, hence, other structures are found in-between.

In Fig. 1 we showcase the relative electronic energies with ZPVE corrections (E_{rel}^{+ZPVE}) for the isomers excluding the Transition State structures (C12 and C13). With the inclusion of ZPVE correction, isomer A1, with absolute energy $E^{+ZPVE}=-187.726045 E_h$, is the most stable structure of the family with a difference of 0.25 eV with respect to C1. The isomers in Fig. 1 are sorted by their relative energy E_{rel} but it can be noted that the order of C5 and C6 and A5 and C7 are interchanged when considering E_{rel}^{+ZPVE} . This is due to the close energy of these two isomers and the effect of the ZPVE. The absolute energies E^{+ZPVE} of isomers A1, C1, C2, A2, A3 and C3 are within the energy range from -187.73 to -187.69 E_h (around 0.79 eV) showing their potential proton transfer interconvertibility (hydrogen shift) from A1 and C1 to their corresponding derivatives at higher energy, respectively. The possible proton transfer reactions from the two most stable isomers, AAN and MCA, to the isomers subsequent in energy are exhibited in Fig. 2. In this diagram we show that a relatively low energy, computed using the CCSD(T)-F12/cc-pVTZ-F12 (see Fig. 1), is needed to isomerise the species A1 and C1 via a proton transfer reaction. The isomerisation energy from A1 to A2 and from A1 to A3 are 52.10 kJ/mol (0.54 eV) and, 58.86 kJ/mol (0.61 eV), respectively. For the methylcyanamide derivatives, the formation of isomer C3 proceeds through two sequential steps: C1 → C2 (first proton transfer) and C2 → C3 (second proton transfer). The isomerization energies associated with these transformations are 15.44 kJ/mol (0.16 eV) and 52.10 kJ/mol (0.54 eV), respectively.

Label	A1	C1	C2	A2	A3	C3
Elec. g.s. (P.G.)	${}^1A'$ (C_s)	1A (C_1)	1A (C_1)	1A_g (C_{2h})	${}^1A'$ (C_s)	${}^1A'$ (C_s)
E_{rel} (cm $^{-1}$)	0.00	2177.7	3468.2	4392.5	4920.0	6533.1
ZPVE (cm $^{-1}$)	13979.87	13796.61	13524.24	13817.02	13728.13	13644.07
E_{rel}^{+ZPVE} (cm $^{-1}$)	0.00	1994.44	3012.57	4229.64	4668.26	6197.30
μ (D)	2.85	5.00	3.40	0.00	3.00	3.58
Label	A4	C4	C5	C6	A5	C7
Elec. g.s. (P.G.)	1A (C_1)	1A (C_1)	1A (C_1)	1A_g (C_{2h})	1A (C_1)	${}^1A'$ (C_s)
E_{rel} (cm $^{-1}$)	10001.3	10323.9	12293.4	12297.5	14025.9	14356.7
ZPVE (cm $^{-1}$)	13603.47	13795.29	13842.91	13439.30	13449.18	13432.06
E_{rel}^{+ZPVE} (cm $^{-1}$)	9624.90	10139.32	12156.67	11756.93	13889.17	13808.89
μ (D)	2.60	3.87	3.31	Nonpolar	1.70	3.22
Label	C8	C9	C10	C11	C12	C13
Elec. g.s. (P.G.)	1A (C_1)	1A (C_1)	1A (C_1)	1A (C_1)	1A_g (D_{2h})	${}^1A'$ (C_s)
E_{rel} (cm $^{-1}$)	15283.2	18389.4	21634.6	31939.5	51780.8	-
ZPVE (cm $^{-1}$)	13465.86	13355.03	13609.84	12846.72	-	-
E_{rel}^{+ZPVE} (cm $^{-1}$)	14769.19	17764.56	21264.57	30806.35	-	-
μ (D)	3.13	4.01	0.92	2.38	Nonpolar	3.99

Figure 1. Isomers of the formula $C_2H_4N_2$, ranked by increasing relative energy E_{rel} (in cm $^{-1}$), referred to the most stable isomer (A1). Their electronic ground states (g.s.), point groups (P.G.), zero-point vibrational energies ZPVE (in cm $^{-1}$), relative energies including the ZPVE corrections E_{rel}^{+ZPVE} (in cm $^{-1}$), and dipole moments μ (in Debye) are also shown. These calculations were carried out with the level of theory CCSD(T)-F12/cc-pVTZ-F12. The pairs A2 & A3, C6 & C12, C7 & C8, and C10 & C13 are conformers of the same isomer. Transition state structures are highlighted in dotted frames as C12 and C13.

1. Comparison among the levels of theory

To evaluate the performance of the three computational methods—MP2/aug-cc-pVTZ, CCSD(T)-F12/cc-pVTZ-F12, and B3LYP/6-31G(d,p)—introduced in Section II, we compare the relative energies of the eighteen $C_2H_4N_2$ isomers under investigation with respect to the lowest-energy structure A1, the only one characterized spectroscopically and observed in the ISM, e.g., in Sgr B2(N) 14,46 . As shown in Figure 3, all three levels of theory yield consistent energy hierarchy, with only minor variations among them, highlighting their overall agreement in predicting the relative stabilities of the isomers.

In general, B3LYP provides the lowest energy values and the results of MP2 are closer to the ones obtained by

CCSD(T)-F12. In particular, for the species C1, a good agreement is observed between the two levels of theory CCSD(T)-F12/cc-pVTZ-F12 and MP2/aug-cc-pVTZ resulting in a relative energy of 0.27 eV and 0.28 eV, respectively.

MP2 provides results comparable to the higher level method CCSD(T)-F12, showing the effectiveness of MP2 level. Furthermore, when MP2 has a divergent behaviour, it can be corrected by including excitation correction terms as they are implemented in the more robust coupled-cluster approach 47 . Particularly, the triple substitutions treated perturbatively in the coupled cluster (CCSD(T)) was considered a gold standard in quantum chemical calculations due to its high accuracy 30 . However, the method with the highest accuracy adopted in this study is the explicitly correlated (F12)

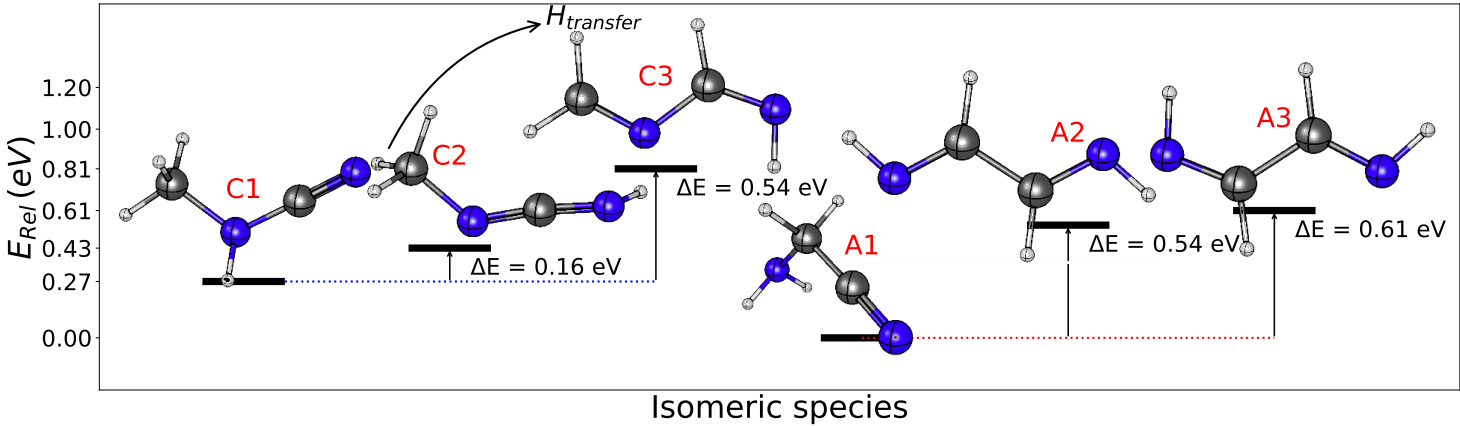


Figure 2. Proton transfer energy diagram of the two most stable isomers of $\text{C}_2\text{H}_4\text{N}_2$ with their relative energies obtained from CCSD(T)-F12/cc-pVTZ-F12. Aminoacetonitrile derivatives are labeled as A_n while cyanomethylamine derivatives as C_n .

coupled cluster (CCSD(T)-F12). This method is based on the gold standard and includes germinal basis functions, i.e., a small set of two-particle basis functions that depends explicitly on the inter-electronic distances and looks almost like the correlation holes. CCSD(T)-F12 has the advantage of requiring not so large basis sets than for the CCSD(T) as well as it is relatively faster and can be used to predict energy and other chemical properties with a high accuracy^{48,49}.

In general, MP2 slightly overestimates the energies with respect to those of CCSD(T)-F12 whereas B3LYP underestimates them. From now on, CCSD(T)-F12 and MP2 will be used, besides estimating the energies, to determine the structure of the isomers especially when high accuracy is needed.

B. Structural and Spectroscopic parameters

1. Structural parameters

Table 1 presents the equilibrium structural parameters of selected $\text{C}_2\text{H}_4\text{N}_2$ isomers optimized at the CCSD(T)-F12/cc-pVTZ-F12 level of theory. Reported values include bond lengths (in Å) and bond angles (in degrees) for the global minimum structure A1, as well as for the two next-lowest-energy aminoacetonitrile derivatives, A2 and A3.

We have calculated the equilibrium internal coordinates for A1 to validate the *ab initio* level of theory used here by comparing them with the experimental and other *ab initio* results. It can be noted that the agreement is rather good except for the bond angles $\angle(\text{C1-C5}\equiv\text{N8})$ and $\angle(\text{H2-C1-H3})$. On the one hand, the value of $\angle(\text{C1-C5}\equiv\text{N8})$ has a discrepancy of about 5° in comparison with the CBS+CV result. Its experimental value was assumed to be fixed at 180°. On the other hand, angle $\angle(\text{H2-C1-H3})$ differs from the experimental value around 5°. This last difference can be explained because its experimental determination assumed the interbond angle $\angle(\text{C1-C5}\equiv\text{N8})$ as 180°. In Table 2, the geometry of the three lowest energy cyanomethylamine derivatives C1, C2 and C3 are given. The geometry of the most stable cyanomethylamine derivative C1 is compared with the available experimental interbond angles, which were determined assuming the equilibrium bond lengths $r(\text{C7}\equiv\text{N8})$ and $r(\text{N5-C7})$ from another molecule with a similar configuration¹⁶. To provide a further comparison, we have also included in Table 2 the equilibrium bond lengths and interbond angles, computed at the level of theory B3LYP/aug-cc-pVTZ, of the molecule $\text{CH}_3\text{NH}_2\text{CN}$ at the electronic state ^2A , which is prone to lose one hydrogen of radical NH_2 ⁵⁰. For this latter case, there is only inconsistency for the $\angle(\text{N5-C7}\equiv\text{N8})$. In general, there is a good agreement of our calculated parameters with the experimental and theoretical work. In addition, we include the equilibrium structure of the other isomers with higher electronic energy in supplementary information tables: (see Tables S1 and S2).

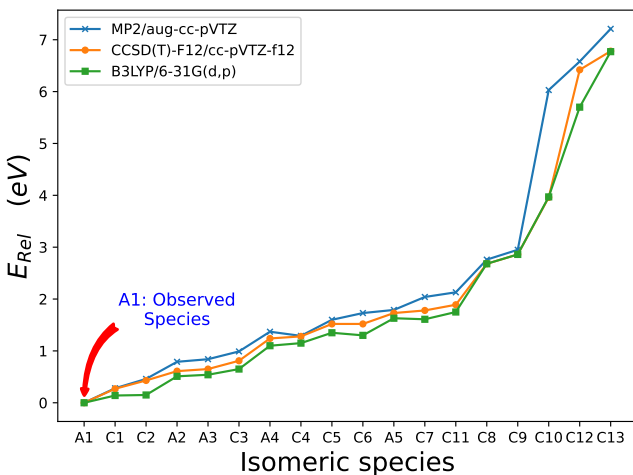


Figure 3. Comparison of the relative energies E_{rel} (in eV) calculated with MP2/aug-cc-pVTZ, CCSD(T)-F12/cc-pVTZ-F12, and B3LYP/6-31G(d,p) methods across 18 isomeric species. The relative energies are given with respect to the value of the most stable isomer A1.

Table 1. Equilibrium geometric parameters (bond lengths in Å and bond angles in degrees) computed at the CCSD(T)-F12/cc-pVTZ-F12 level for the first A1, A2, and A3 isomers of $C_2H_4N_2$.

A1				A2		A3	
Description	This work	Exp. ^a	CBS+CV ^b	Description	This work	Description	This work
R(C5≡N8)	1.171	1.1594(44)	1.156	R(H3N1)	1.020	R(H3N1)	1.024
R(C1C5)	1.474	1.4611(40)	1.476	R(N1C2)	1.281	R(N1C2)	1.281
R(C1H2)	1.089	1.0940(48)	1.088	R(C2H4)	1.098	R(C2H4)	1.087
R(C1H3)	1.089			R(C2C5)	1.477	R(C2C5)	1.474
R(N4H6)	1.013	1.0138(30)	1.010	R(C5H6)	1.098	R(C5H6)	1.095
R(N4-H7)	1.013			R(C5N7)	1.276	R(C5N7)	1.279
R(C1N4)	1.456	1.4760(40)	1.452	R(N7H8)	1.024	R(N7H8)	1.020
∠(C1-C5≡N8)	177.39	180.0	182.2	∠(H3N1C2)	110.5	∠(H3N1C2)	109.82
∠(N4-C1-C5)	114.79	114.54(28)	114.80	∠(H4C2C5)	114.77	∠(H4C2C5)	115.77
∠(C1N4H6)	110.24	109.6(5)	110.5	∠(H6C5C2)	114.8	∠(H6C5C2)	116.12
∠(C1N4H7)	110.24			∠(H8N7C5)	110.50	∠(H8N7C5)	110.49
∠(H2C1H3)	107.06	102.4(19)		∠(C2C5N7)	119.40	∠(C2C5N7)	119.53
∠(H6N4H7)	106.76	107.3(14)		∠(H4C2N1)	125.90	∠(H4C2N1)	119.09

^a Experimental structural parameters for A⁴³ has been included for validating our results. We have considered the largest uncertainties determined. The angle given without uncertainty is assumed.

^b *Ab initio* geometric parameters obtained at the Complete Basis Set (CBS) limit including the core-valence correlation (CV)⁵¹. The extrapolation was carried out using the levels of theory fc-CCSD(T)/cc-pVnZ level, with n = T and Q, and CCSD(T)/cc-pCVTZ within the fc approximation and correlating all electrons.

Table 2. Equilibrium geometric parameters (bond lengths in Å and bond angles in degrees) computed at the CCSD(T)-F12/cc-pVTZ-F12 level for the first C1, C2, and C3 isomers of $C_2H_4N_2$.

C1			C2		C3	
Description	This work	Exp. ^a	Description	This work	Description	This work
R(C7≡N8)	1.175		R(C2N3)	1.453	R(H1C2)	1.093
R(N5C7)	1.344		R(N3C4)	1.218	R(H3C2)	1.417
R(C1N5)	1.467		R(C4N7)	1.237	R(N3N4)	1.279
R(N5H6)	1.009		R(N7H8)	1.012	R(C4H5)	1.094
R(C1H3)	1.009		R(C2H1)	1.089	R(C4H6)	1.084
R(C1H2)	1.086		R(C2H5)	1.087	R(N7C2)	1.271
R(C1H4)	1.086		R(C2H6)	1.088	R(N6H8)	1.023
∠(N5C7≡N8)	176.85	179.92	∠(C2N3C4)	128.05	∠(H1C2N3)	116.95
∠(C1N5C7)	116.18	112.90	∠(N3C4N7)	170.39	∠(H1C2N7)	119.34
∠(N5C1H4)	108.21		∠(C4N7H8)	117.23	∠(C2N3C4)	114.84
∠(H4C1H3)	109.68		∠(N3C2H1)	112.22	∠(N3C2N7)	123.70
∠(H6N5C7)	112.69		∠(H1C2H6)	109.33	∠(H8N7C2)	108.37
∠(H6N5C1)	114.54		∠(N3C2H5)	108.66	∠(N4C5H7)	119.09

^a Experimental coordinates determined assuming r(C7≡N8)=1.160 Å and r(N5C7)=1.400 Å¹⁶.

2. Harmonic and Anharmonic vibrational Frequencies

The fundamental frequencies of isomers $C_2H_4N_2$ from A1 to C11, ruling out the transition states C12 and C13, have been calculated using two levels of theory, CCSD(T)/cc-pVTZ and MP2/aug-cc-pVTZ. The harmonic frequencies are computed in this work at the level of theory CCSD(T)/cc-pVTZ. The anharmonic vibrational frequencies are obtained using

$$E = \sum_i \omega_i^{\text{CCSD(T)}} \left(\nu_i + \frac{1}{2} \right) + \sum_{i \geq j} x_{ij}^{\text{MP2}} \left(\nu_i + \frac{1}{2} \right) \left(\nu_j + \frac{1}{2} \right) \quad (2)$$

where ω_i are the harmonic fundamentals, ν_i and ν_j are vibrational quanta, and x_{ij} are the anharmonic parameters. The harmonic contribution at CCSD(T)/cc-PVTZ level is corrected

with the anharmonic constants derived using MP2/AVTZ force field, as implemented in Refs.^{52,53}

In Table 3 we present the harmonic CCSD(T)/cc-pVTZ fundamentals and the anharmonic ones calculated with Eq. (2) of aminoacetonitrile (A1), with their vibrational mode descriptions, and of its derivatives A2 and A3. Isomer A1 has been included here as a benchmark of the values computed for the new species in this work. The results obtained for A1 are compared with the experimental vibrational frequencies and the theoretical anharmonic frequencies, denoted as CBS+CV/MP2, obtained at the complete basis set (CBS) limit including the core-valence correlation (CV) and corrected with anharmonic contributions at the ae-MP2/cc-pCVTZ level⁵¹. The structure of isomer A1 has a point group C_s . This group characterises the first 11 vibrational modes with an irreducible representation A' and the other 7 modes

with a symmetry A'' . From the experimental data, seven of the lowest fundamental frequency have been measured with high resolution techniques^{14,51} and low resolution experimental data of other 10 fundamental frequencies were also reported⁵⁴. In general, our anharmonic frequencies calculated with Eq. (2) have a good agreement (within a few cm^{-1}) with their corresponding experimental values and CBS+CV/MP2 results. Nevertheless, large discrepancies with respect to the experimental frequencies are found between 40-90 cm^{-1} for the modes ν_2 , ν_3 , ν_4 and ν_9 . Interestingly, the harmonic frequencies ω_3 , ω_4 , and ω_9 at CCSD(T)/cc-PVTZ level are closer to the experimental frequencies than the anharmonic ones.

The low-lying A2 conformer belongs to the C_{2h} point group. Thus, the A2 conformer exhibits nine Raman-active modes ($7A_g + 2B_g$) and nine IR-active modes ($3A_u + 6B_u$) as arranged in descending order on the tables. The A_u modes correspond to dipole oscillations along the z -axis, whereas the B_u modes involve dipole components in the molecular xy plane. All irreducible representations of C_{2h} are one-dimensional; therefore, all vibrational modes are nondegenerate. These symmetry assignments were confirmed by inspection of the computed normal mode displacements. A comparison of the A2 vibrational modes analyzed, (ν_1 , ν_3 , ν_4 , ν_5 , ν_{13} , ν_{15} , ν_{16} , ν_{17}) show excellent agreement (within 10 cm^{-1}) between the anharmonic (this work) and F12-TcCR+DZ levels¹⁸, all other modes have very good consistency. Low-frequency bending or torsional modes ($<600 \text{ cm}^{-1}$) exhibit larger relative deviations, typical of floppy or coupled vibrations. The A3 conformer adopts C_s symmetry, leading to two irreducible representations: A' (symmetric with respect to the mirror plane) and A'' (antisymmetric). Accordingly, the first eleven modes are of A' symmetry, whereas modes 12–18 correspond to A'' . Both representations are IR and Raman active, with A' modes polarized in the molecular plane and A'' modes polarized perpendicular to it. A comparison of our vibrational frequencies of A2 and A3 with other *ab initio* calculations, corresponding to the conformers anti-(E,E) and anti-(E,Z), respectively¹⁸, shows a good agreement. The calculations given in Ref.¹⁸ resulted from a harmonic frequency analysis computed at CCSD(T)-F12b/cc-pCVTZ-F12 level of theory with relativistic corrections and the anharmonic analysis at CCSD(T)-F12/cc-pVDZ¹⁸.

Table 4 presents the harmonic CCSD(T)/cc-pVTZ fundamentals and the anharmonic frequencies calculated with Eq. (2) of methylcyanamide (C1), along with their vibrational mode descriptions, as well as those from its derivatives C2 and C3. The structures of C1 and C2 have a point group, C_1 and, therefore, all their vibrational modes are totally symmetric. Isomer C3 has a symmetry, C_s and their first 13 vibrational modes are A' and other 5 (from 14th to 18th) vibrational modes are A'' . For C1 conformer, Bak and Svanholt reported an "approximate" experimental frequency of 105 cm^{-1} for ν_{18} mode, closer to the theoretical frequency of 95 cm^{-1} in our work. The harmonic (ω_i) and anharmonic (ν_i) fundamental frequencies for the 6 lowest energy isomers A1, A2, A3, C1, C2 and C3 computed at MP2/aug-cc-pVTZ level of theory are given in Table 5. Resonances in Tables 3, 4, and 5 were de-

termined from the energy separations between anharmonic vibrational states within about $30 \pm 5 \text{ cm}^{-1}$ following Ref.⁵⁵.

In the supplementary information, the harmonic vibrational frequencies at the level of theory CCSD(T)/cc-pVTZ with the anharmonic MP2/aug-cc-pVTZ corrections calculated with Eq. (2), and the harmonic and anharmonic fundamentals at the level of theory MP2/aug-cc-pVTZ are provided for the isomers with higher electronic energy from A4, omitting the transition states C12 and C13. In Tables S3 and S4, the CCSD(T)/cc-pVTZ harmonic frequencies and the anharmonic fundamentals calculated with Eq. (2) are reported. Table S5 presents the harmonic and anharmonic fundamentals at the level of theory MP2/aug-cc-pVTZ of A4, C4, C5, C6, A5, C7, C8, C9, C10 and C11 isomers.

3. Spectroscopic parameters and dipole moments

The spectroscopic constants of the family of isomers $\text{C}_2\text{H}_4\text{N}_2$ are also made available. In this section, we pay special attention to the spectroscopic constants of the energy lowest aminoacetonitrile derivatives A1, A2 and A3 and cyanomethylamine derivatives C1, C2 and C3 as well as providing their dipole moments. The $\text{C}_2\text{N}_2\text{H}_4$ is a polar molecule and exhibits closely spaced conformers, diffuse functions³⁵ may influence geometries and relative energies. Due to this, geometry optimizations and harmonic frequencies were performed at the MP2/aug-cc-pVTZ level to include diffuse functions for structural description and ZPE corrections. Electronic reference energies were computed at the CCSD(T)-F12/cc-pVTZ-F12 level; the F12 approach accelerates basis-set convergence, providing near-CBS energies without requiring augmented F12 basis sets, which are less standardized and can introduce numerical issues²⁶. Selected CCSD(T)/cc-pVTZ single-points were employed to validate the protocol. A first comparison of the equilibrium rotational constants and the total dipole moments of the six lowest energy isomers is showed in Table 6 using three *ab initio* levels of theory MP2/aug-cc-pVTZ, CCSD(T)/cc-pVTZ and CCSD(T)-F12/cc-pVTZ-F12. It can be noted that, in general, the equilibrium rotational constants obtained from MP2/aug-cc-pVTZ and CCSD(T)/cc-pVTZ using Gaussian are closer for some species like A2, C1. The values obtained from CCSD(T)-F12/cc-pVTZ-F12 using Molpro was added for qualitative comparison even though computationally its convergence thresholds differ. However, the general agreement shows how reliable these methods are in computing geometric parameters for similar molecular species.

In Table 6 we also present the ground vibrational state rotational constants. These were computed using the equilibrium rotational constants from CCSD(T)-F12/cc-pVTZ-F12 and the vibrational contribution ΔB^{vib} derived from the vibration-rotation interaction parameters determined from the MP2/AVTZ force field:

$$B_0 = B_e(\text{CCSD(T)-F12/VTZ-F12}) + \Delta B^{\text{vib}}(\text{MP2/AVTZ}) , \quad (3)$$

Table 3. Harmonic fundamental vibrational frequencies at the CCSD(T)/cc-pVTZ level of theory and the anharmonic frequencies calculated with Eq. (2) (both in cm^{-1}) for the isomers A1, A2 and A3.

Vib. Mode	A1				A2				A3						
	This Work Harm. Fr	This work Anharm.	Exp. Freq. ^a	CBS + CV/MP2 ^d	Description	Type of Vibration (Γ_{vib})	Harm Freq	Anharm Freq	Exp. ^e	F12- TcCR+DZ ^f	Γ_{vib}	Harm Freq	Anharm Freq	F12- TcCR+ DZ ^f	Γ_{vib}
ν_1	3518	3377	3367(1)	3378	H6-N4-H7	Sym. stre (A')	3465	3301		3303	A_g	3417	3252	3303	A'
ν_2	3092	2993	2950(1)	2952	H2-C1-H3	Sym. stre (A')	3101	2948		2925	A_g	3339	3169	3239	A'
ν_3	2228	2185	2236(1)	2254	C5≡N8	Stretching (A')	1700	1652		1652	A_g	3157	3023	2992	A'
ν_4	1673	1549	1642(1)	1617	H6-N4-H7	Bending (A')	1428	1392		1386	A_g	3014	2857	2881	A'
ν_5	1478	1451	1444(1)	1446	H2-C1-H3	Bending (A')	1276	1249		1248	A_g	1684	1638	1645	A'
ν_6	1369	1334	1348(1)	1338	H2-C1-H3	Wagging (A')	1021	997		975	A_g	1625	1601	1616	A'
ν_7	1126	1086	1077(1)	1086	C1-N4	Stretching (A')	586	578		565	A_g	1406	1371	1381	A'
ν_8	946	910	901.4(1) ^b	898	C1-C5	Stretching (A')	1128	1099		1083	A_u	1379	1347	1361	A'
ν_9	846	719	790.95908(7) ^b	811	H6-N4-H7	Wagging (A')	651	634	646	603	A_u	1278	1249	1259	A'
ν_{10}	571	566	556.56467(2) ^b	559	C1-C5-N8	Bending (A')	169	165		78	A_u	1171	1146	1159	A'
ν_{11}	235	235	210.575841(5) ^c	211	N4-C1-C5	Bending (A')	1103	1081		1056	B_g	1029	1004	996	A'
ν_{12}	3604	3437	3431(1)	3448	H6-N4-H7	Asym. stre (A'')	909	891		878	B_g	573	566	558	A'
ν_{13}	3136	2994	2975(1)	2991	H2-C1-H3	Asym. Stre (A'')	3465	3301		3301	B_u	350	353	348	A'
ν_{14}	1395	1355	1331(1)	1360	H ₂ C1-H ₂ N4	Twisting (A'')	3101	2985	3114	2928	B_u	1151	1124	1107	A''
ν_{15}	1200	1174	1160(1) ^b	1173	H2-C1-H3	Twisting (A'')	1640	1612	1604	1613	B_u	1112	1092	1074	A''
ν_{16}	890	881	—	884	H2-C1-H3	Rocking (A'')	1377	1350		1345	B_u	918	905	895	A''
ν_{17}	392	385	368.104656(3) ^c	370	C1-C5-N8	Bending (A'')	1176	1152	1155	1149	B_u	668	652	628	A''
ν_{18}	261	254	244.891525(3) ^c	248	H6-N4-H7	Torsion (A'')	337	339		324	B_u	186	186	148	A''

^a Low resolution data of the experimental fundamental frequencies⁵⁴. When available, high resolution experimental frequencies are given instead.

^b High resolution experimental fundamentals measured by Jiang *et al.*⁵¹.

^c High resolution experimental fundamentals obtained by Melosso *et al.*¹⁴.

^d *Ab initio* anharmonic frequencies, denoted as CBS + CV/MP2, obtained at the Complete Basis Set (CBS) limit including the core-valence correlation (CV) and corrected with anharmonic contributions at the ae-MP2/ cc-pCVTZ level⁵¹. The CBS extrapolation was carried out using the levels of theory fc-CCSD(T)/cc-pVnZ level, with n = T and Q, and CCSD(T)/cc-pCVTZ within the fc approximation and correlating all electrons.

^e Experimental Ar-matrix results from Ref.⁵⁶

^f Calculations from Ref.18, named as F12-TcCR+DZ, resulted from a harmonic contribution computed at the level of theory CCSD(T)-F12b/cc-pCVTZ-F12 with relativistic corrections and the anharmonic one at CCSD(T)-F12/cc-pVDZ.

Only interactions between the anharmonic vibrational bands whose energy separation is within about $30 \pm 5 \text{ cm}^{-1}$ were treated as significant.
; A1: $\nu_{15} \leftrightarrow \nu_8 + \nu_{18}$, A2: $\nu_{14} \leftrightarrow \nu_{16} + \nu_3$, $\nu_{15} \leftrightarrow \nu_{18} + \nu_5$, $\nu_{16} \leftrightarrow \nu_{18} + \nu_6$. A3: $\nu_6 \leftrightarrow \nu_9 + \nu_{13}$.

which is applied for the three rotational constants A_0 , B_0 and C_0 . To assess these results, next we compare the theoretical rotational constants from Eq. (3) with the available experimental ground state rotational constants, i.e., those from aminoacetonitrile A1 and methylcyanamide C1. The experimental ground state rotational constants of aminoacetonitrile A1 are $A_0=30246.4909(9)$ MHz, $B_0=4761.0626(1)$ MHz and $C_0=4310.7486(1)$ MHz⁵¹. Our calculations provided the differences about 247 MHz, 26 MHz and 26 MHz, respectively. For methylcyanamide C1 (or MCA), the experimental ground state rotational constants fitted for the transitions with symmetry $a+$ are $A_0=36090(156)$ MHz, $B_0=4977.13(7)$ MHz and $C_0=4505.13(7)$ MHz¹⁶. Our calculations from Eq. (3) differ to be about 1109 MHz, 16 MHz and 20 MHz, respectively. It should be noted that the experimental-calculated difference of ΔA is very large. Nevertheless, the comparison of the theoretical with the experimental value of A_0 is less definitive because its experimental rotational constant has a substantial uncertainty whereas B_0 and C_0 are well determined. In addition, this large difference can also arise from the fact that the experimental rotational constants were estimated only from a fit of a few transitions with symmetry either $a+$ or $a-$ ¹⁶. MCA

has two large amplitude motions which splits each rotational transition into four, labeled as $a+$, $a-$, $e+$ and $e-$. The values of B_0 and C_0 for both symmetries $a+$ and $a-$ are similar but the values of A_0 are rather different. According to this comparison, a new measurement of the experimental spectrum of MCA would be convenient to determine the constant A_0 with accuracy.

Concerning the results of the total dipole moments given in Table 6, the two methods (MP2 and CCSD(T)) are in good accordance, with dipole moment predictions. For instance, A1 has 2.54 and 2.85 D at MP2/AVTZ and CCSD(T)/cc-pVTZ respectively while experimentally it was determined to be 2.64 D. The A2 isomer has a dipole moment of 0.00 D due to its molecular symmetry. In contrast, the MCA isomer exhibits a dipole moment of 5.04 D at the MP2 level, in close agreement with the CCSD(T). MP2 values are generally lower compared to CCSD(T), widely considered gold standard in quantum chemical calculations³⁰. The dipole moments of these five isomers (A1, A3, C1, C2 and C3) are relatively large and, according to these values, they are potentially observable species either in the atmosphere or the interstellar medium. The isomer A2 does not have dipole moment.

Table 4. Harmonic vibrational frequencies at the CCSD(T)/cc-pVTZ level of theory and the anharmonic frequencies computed with Eq. (2) (both in cm^{-1}) for the isomers C1, C2 and C3.

Vib.	MCA(C1)				C2		C3	
	Mode	Harm. Freq	Anharm Freq	Description	Type of vibration	Harm Freq	Anharm Freq	Harm Freq
ν_1	3594	3436	N5-H6	Stretching	3575	3412	3435	3269
ν_2	3176	3038	H2-C1-H4	Asym. str.	3129	2991	3183	3047
ν_3	3144	3008	CH ₃	Asym. str.	3120	2981	3070	2910
ν_4	3060	2937	CH ₃	Sym. str.	3040	2981	3036	2890
ν_5	2245	2210	N5-C7-N8	Stretching	2202	2149	1684	1646
ν_6	1526	1480	CH ₃	Asym. bending	1516	1506	1667	1624
ν_7	1501	1471	CH ₃	Asym. bending	1501	1472	1485	1451
ν_8	1469	1452	N5-H6	Twisting/bending	1454	1436	1413	1380
ν_9	1457	1416	CH ₃	Sym. bending	1367	1344	1281	1250
ν_{10}	1196	1177	CH ₃	Wagging	1144	1116	1213	1188
ν_{11}	1165	1139	C7-N5	Stretching	1143	1119	985	957
ν_{12}	1146	1132	CH ₃	Rocking	981	908	605	594
ν_{13}	936	926	H4-C1-N5	Bending	905	880	364	362
ν_{14}	656	602	N5-C7-N8	Bending	644	636	1107	1083
ν_{15}	544	516	N5-C7-N8	Bending	586	568	1070	1054
ν_{16}	443	420	N5-H6	Inversion	473	459	920	903
ν_{17}	227	224	C1-N5-C7	Bending	197	193	647	626
ν_{18}	110	95	CH ₃	Torsion	74	61	123	118

Only interactions between the anharmonic vibrational bands whose energy separation is within about $30 \pm 5 \text{ cm}^{-1}$ were treated as significant: C1: $\nu_4 \leftrightarrow 2\nu_6$, $\nu_8 \leftrightarrow \nu_{13} + \nu_{15}$, $\nu_{12} \leftrightarrow \nu_{13} + \nu_{17}$. C2: $\nu_4 \leftrightarrow 2\nu_6$, $\nu_7 \leftrightarrow \nu_8 + \nu_{18}$, $\nu_{12} \leftrightarrow 2\nu_{16}$, $\nu_2 \leftrightarrow \nu_3$, $\nu_{10} \leftrightarrow \nu_{11}$. C3: $\nu_{14} \leftrightarrow \nu_{11} + \nu_{18}$.

We should highlight that our results are comparable with others available in the literature¹⁸. For A1 species, the experimental dipole moment is 2.640(7) D⁴³, akin to the calculations obtained for MP2/aug-cc-pVTZ, to be 2.54 D, and the coupled cluster methods CCSD(T)/cc-pVTZ and CCSD(T)-F12/cc-pVTZ-F12 to be 2.85 D and 2.86 D, respectively. A2 with 0.00 D agrees with previous work¹⁸. For A3 isomer, the dipole moment was recently computed via B3LYP/aug-cc-pVTZ to be 2.78 D¹⁸ while our calculations resulted in 2.83 D at MP2/aug-cc-pVTZ and 3.00 D at CCSD(T)/cc-pVTZ. The good agreement in these comparisons supports the reliability of our results.

According to the accuracy provided by the level of theory MP2/aug-cc-pVTZ in Table 6, we have also provided the rotational and centrifugal distortion (quartic and sextic) constants of the S-reduced Watson Hamiltonian at MP2/aug-cc-pVTZ level of theory. In Table 7 we report their values of the isomers A1, A2 and A3 and in Table 8 their values of isomers C1, C2 and C3. On the one hand, a comparison with the available experimental parameters is relevant to estimate the degree of accuracy of the calculations. For aminoacetonitrile (A1 or AAN) species, we obtained $A_0 = 29965.759 \text{ MHz}$, $B_0 = 4739.798 \text{ MHz}$, and $C_0 = 4287.742 \text{ MHz}$ and the difference with the experimental parameters⁵¹ are $\Delta A \approx 281 \text{ MHz}$, $\Delta B \approx 21 \text{ MHz}$, and $\Delta C \approx 23 \text{ MHz}$. For species C1, the experimental-MP2 differences for the rotational constants are $\Delta A \approx 1099 \text{ MHz}$, $\Delta B \approx 14 \text{ MHz}$, and $\Delta C \approx 18 \text{ MHz}$ (see the experimental rotational constants fitted for the transitions with symmetry $a+$ ¹⁶). As for the results given by the Eq. (3), the experimental-calculated difference of ΔA is very large. In both

cases, for A1 and C1, the differences of our MP2 calculations with respect to the experimental values of the rotational constants B_0 and C_0 are between 14 to 23 MHz, close to those obtained with Eq. (3), whereas the differences for A_0 are larger, as it happens in other works^{57,58}.

On the other hand, comparison of our MP2 spectroscopic parameters with higher-level theoretical results¹⁸ is also valuable. McKissick et al. computed the rotational constants as well as the quartic and sextic distortion constants for isomers A2 and A3 at the F12-TcCR+DZ QFF and F12-TcC QFF levels of theory. For isomer A2, the differences between our MP2 parameters and those reported by McKissick et al. are less than 0.5% for the ground-state rotational constants and approximately 2%, 5%, and 0.2% for the quartic distortion constants D_J , D_{JK} , and D_K , respectively. For A3 species, the differences of the ground state rotational constants are of 1.0% for A_0 , 0.1% for B_0 and of 0.3% for C_0 , and about 3%, 0.3%, and 0.08% for D_J , D_{JK} , and D_K .

Results from other isomers with higher electronic energies (A4-C11) are provided in table S6 of the supplementary material. For those, we provided the rotational and centrifugal distortion (quartic and sextic) constants of the S-reduced Watson Hamiltonian, calculated at MP2/aug-cc-pVTZ level of theory.

C. Methylcyanamide (MCA or C1) molecule

The isomer MCA (or C1 in fig. 1) is the second one in energy and has the largest dipole moment among all the isomers of $\text{C}_2\text{H}_4\text{N}_2$ presented in this work (see Fig.1).

Table 5. Harmonic (ω) and anharmonic (ν) fundamental vibrational frequencies (in cm^{-1}) for selected isomers of $\text{C}_2\text{H}_4\text{N}_2$ at MP2/aug-cc-pVTZ level of theory^a

Vibrat. modes	A1	A2	A3	C1	C2	C3
ω_1	3532	3485	3484	3606	3602	3460
ω_2	3108	3116	3429	3199	3175	3220
ω_3	2180	1684	3168	3166	3166	3091
ω_4	1666	1409	3070	3075	3074	3064
ω_5	1490	1277	1673	2229	2219	1674
ω_6	1369	1015	1624	1539	1528	1659
ω_7	1123	585	1405	1516	1516	1486
ω_8	941	1129	1381	1470	1463	1403
ω_9	842	658	1282	1463	1386	1268
ω_{10}	562	165	1177	1200	1153	1201
ω_{11}	209	1102	1023	1165	1146	989
ω_{12}	3625	910	573	1152	937	603
ω_{13}	3159	3485	334	938	898	364
ω_{14}	1395	3117	1145	657	641	1103
ω_{15}	1203	1628	1098	532	564	1074
ω_{16}	894	1364	919	436	466	920
ω_{17}	374	1169	655	214	188	644
ω_{18}	255	338	151	167	64	115
ν_1	3391	3320	3320	3448	3440	3294
ν_2	3010	2962	3260	3062	3037	3084
ν_3	2138	1636	3036	3031	3027	2931
ν_4	1542	1372	2913	2951	3015	2918
ν_5	1463	1250	1626	2195	2166	1635
ν_6	1333	991	1582	1493	1519	1617
ν_7	1083	577	1371	1486	1486	1452
ν_8	905	1101	1349	1453	1445	1370
ν_9	715	641	1253	1421	1362	1237
ν_{10}	557	161	1152	1181	1125	1176
ν_{11}	209	1080	998	1138	1121	962
ν_{12}	3458	902	566	1138	864	592
ν_{13}	3018	3320	337	929	873	362
ν_{14}	1356	3001	1118	603	633	1078
ν_{15}	1178	1600	1078	504	546	1059
ν_{16}	885	1337	906	413	451	903
ν_{17}	367	1145	639	212	185	623
ν_{18}	248	340	149	153	50	109

Only interactions between the anharmonic vibrational bands whose energy separation is within about $30 \pm 5 \text{ cm}^{-1}$ were treated as significant: A1 $\nu_7 \leftrightarrow 2\nu_{10}$, $\nu_{15} \leftrightarrow \nu_8 + \nu_{18}$.

A2: $\nu_{16} \leftrightarrow \nu_6 + \nu_{18}$, $\nu_{15} \leftrightarrow \nu_5 + \nu_{18}$, $\nu_{14} \leftrightarrow \nu_3 + \nu_{16}$.

A3: $\nu_6 \leftrightarrow \nu_9 + \nu_{13}$.

C1: $\nu_4 \leftrightarrow 2\nu_6$, $\nu_8 \leftrightarrow \nu_{13} + \nu_{15}$, $\nu_{12} \leftrightarrow \nu_{13} + \nu_{17}$.

C2: $\nu_7 \leftrightarrow \nu_8 + \nu_{18}$, $\nu_4 \leftrightarrow 2\nu_6$, $\nu_2 \leftrightarrow \nu_3$, $\nu_{10} \leftrightarrow \nu_{11}$.

C3: $\nu_{14} \leftrightarrow \nu_{11} + \nu_{18}$.

MCA is a near prolate asymmetric top with an asymmetry parameter $\kappa = \frac{2B_0 - A_0 - C_0}{A_0 - C_0} = -0.969$ computed with the ground state rotational constants reported in Table 6. Its equilibrium structure at the level of theory CCSD(T)-F12/cc-pVTZ-F12 is given in Table 2, and illustrated in Fig. 4. The total dipole moment of MCA, computed at the level of theory CCSD(T)-F12/cc-pVTZ-F12, is the largest one (5.04 D) of the family $\text{C}_2\text{H}_4\text{N}_2$ and its dipole components were computed to be $\mu_a = 4.85$ D, $\mu_b = -1.08$ D, and $\mu_c = 0.89$ D, in good agreement with the two available experimental components $\mu_a = 4.72$ D

Table 6. Comparison of the equilibrium rotational constants (in MHz) and total dipole moments μ (in Debye) of the isomers A1, A2, A3, C1, C2, and C3 among the three *ab initio* methods MP2/aug-cc-pVTZ, CCSD(T)/cc-pVTZ and CCSD(T)-F12/cc-pVTZ-F12

Para.	MP2/ AVTZ	Ground			Previous rotational constants
		CCSD(T)	CCSD(T)-F12	State	
A1					
A_e	30063.98	30109.31	30097.70	29999.50	$A_0 = 30248.57(70)^a$ $30246.49(9)^d$
B_e	4764.54	4761.76	4760.24	4735.50	$B_0 = 4760.93(60)^a$ $4761.06(1)^d$
C_e	4314.79	4313.45	4311.99	4284.94	$C_0 = 4310.77(60)^a$ $4310.75(1)^d$
μ	2.54	2.85			2.64 ^a
A2					
A_e	51213.62	51213.62	51352.20	50603.54	$A_0 = 50971.20^b$
B_e	4686.86	4686.86	4669.43	4658.24	$B_0 = 4674.90^b$
C_e	4293.90	4293.90	4280.23	4265.92	$C_0 = 4282.5^b$
μ	0.0	0.00			0.00 ^b
A3					
A_e	48828.47	49369.58	48807.93	48261.72	48398.40^b
B_e	4682.14	4647.39	4680.73	4650.73	4677.10^b
C_e	4272.45	4247.60	4271.12	4242.75	4265.70^b
μ	2.83	3.00			2.78 ^b
C1					
A_e	34943.27	34943.27	34932.44	34980.64	$A_0 = 36090.00(156)^c$
B_e	4997.71	4997.71	4995.31	4960.74	$B_0 = 4977.13(7)^c$
C_e	4522.44	4522.44	4520.30	4485.15	$C_0 = 4505.13(7)^c$
μ	5.04	5.00			
C2					
A_e	54322.08	53951.25	54307.01	55229.14	
B_e	4477.51	4403.89	4475.39	4441.88	
C_e	4296.35	4228.78	4294.32	4237.00	
μ	2.37	3.40			
C3					
A_e	50149.97	49861.33	50131.85	49594.88	
B_e	5072.00	5061.12	5069.54	5028.51	
C_e	4606.15	4594.74	4603.97	4569.51	
μ	3.09	3.58			

^a Experimental ground state rotational constants by Ref.⁴³.

^b Calculated rotational constants and dipole moments for A2 and A3 computed using the F12-TcCR+DZ and F12-TcC QFFs, respectively by Ref.¹⁸.

^c Experimental rotational constant of MCA (a+ symmetry) with assumed geometry from a related molecule with similar skeleton (CH_3NHCl).

^d Experimental ground state rotational constants by Ref.⁵¹

and $\mu_b = 1.30$ D¹⁶.

MCA has 18 vibrational modes, of which at least two of them are large amplitude motions: the methyl internal rotation (ν_{18}) and the inversion motion H6-N5 (ν_{16}). The Table 4 shows the harmonic and anharmonic contributions obtained at CCSD(T)/cc-PVTZ and MP2/AVTZ force field, respectively. The methyl group is an internal rotor with a frequency of 95 cm⁻¹ and the inversion mode has a frequency of 420 cm⁻¹. These two large-amplitude modes split each rotational transition into four, hindering spectral characterization (see Ref.¹⁶).

Table 7. Rotational and centrifugal distortion (quartic and sextic) constants of A1, A2, and A3 calculated at MP2/aug-cc-pVTZ level of theory

Mol. Sym	Rotational Constants (MHz)		Centrifugal Distortion Constants Watson S reductions	
	Equilibrium	g.s.	Quartic terms (kHz)	Sextic terms (Hz)
A1	$A_e=30063.977$	$A_0=29965.759$	$D_J=3.1319$	$H_J=0.0105$
	$B_e=4764.538$	$B_0=4739.798$	$D_{JK}=-60.2600$	$H_K=-83.7900$
	$C_e=4314.793$	$C_0=4287.742$	$D_K=723.1999$	$H_{JK}=-0.9714$
			$d_1=-0.6935$	$H_{KJ}=14.7300$
			$d_2=-0.02732$	$h_1=0.0036$
				$h_2=-0.0003$
				$h_3=0.0000$
A2	$A_e=51213.618$	$A_0=50626.262$	$D_J=0.0009$	$H_J=0.0001$
	$B_e=4686.857$	$B_0=4659.622$	$D_{JK}=-0.0076$	$H_K=4.612$
	$C_e=4293.897$	$C_0=4267.255$	$D_K=0.3581$	$H_{JK}=-0.0254$
			$d_1=-0.0001$	$H_{KJ}=-0.1639$
			$d_2=-0.4568D-05$	$h_1=0.0000$
				$h_2=0.0000$
				$h_3=0.0000$
A3	$A_e=48828.471$	$A_0=48282.260$	$D_J=0.9608$	$H_J=0.00009$
	$B_e=4682.136$	$B_0=4652.139$	$D_{JK}=-6.8340$	$H_K=4.7610$
	$C_e=4272.453$	$C_0=4244.087$	$D_K=312.8000$	$H_{JK}=-0.0149$
			$d_1=-0.1089$	$H_{KJ}=-0.3547$
			$d_2=-0.0054$	$h_1=0.0000$
				$h_2=0.0000$
				$h_3=0.0000$

Table 8. Rotational and centrifugal distortion (quartic and sextic) constants of C1, C2 and C3 calculated at MP2/aug-cc-pVTZ level of theory

Mol sym	Rotational Constants (MHz)		Centrifugal Distortion Constants Watson S reduction	
	Equilibrium	g.s.	Quartic terms (kHz)	Sextic terms (Hz)
C1	$A_e=34943.268$	$A_0=34991.465$	$D_J=3.043$	$H_J=0.9714D-02$
	$B_e=4997.712$	$B_0=4963.140$	$D_{JK}=-73.19$	$H_K=0.7418D+02$
	$C_e=4522.437$	$C_0=4487.285$	$D_K=1219.000$	$H_{JK}=-0.49919$
			$d_1=-0.6842$	$H_{KJ}=-4.514$
			$d_2=-0.01828$	$h_1=0.3963D-02$
				$h_2=0.3608D-03$
				$h_3=0.1045D-03$
C2	$A_e=54322.084$	$A_0=55244.215$	$D_J=2.392$	$H_J=0.7589D-02$
	$B_e=4477.514$	$B_0=4444.001$	$D_{JK}=-126.9$	$H_K=0.2436D+04$
	$C_e=4296.351$	$C_0=4267.693$	$D_K=6947.000$	$H_{JK}=-1.572$
			$d_1=-0.4241$	$H_{KJ}=-256.3$
			$d_2=0.04162$	$h_1=0.2627D-02$
				$h_2=-0.3920D+02$
				$h_3=0.1084D+01$
C3	$A_e=50149.968$	$A_0=49613.003$	$D_J=1.0530$	$H_J=-0.1031D-03$
	$B_e=5072.001$	$B_0=5030.971$	$D_{JK}=-6.568$	$H_K=0.5992D+01$
	$C_e=4606.150$	$C_0=4571.691$	$D_K=379.0000$	$H_{JK}=-0.0175$
			$d_1=-0.1258$	$H_{KJ}=-0.4463$
			$d_2=-0.1258$	$h_1=0.1563D-04$
				$h_2=0.3651D-05$
				$h_3=0.1039D-05$

An analysis of the torsional potential surface and its correlation with the N-H inversion angles is critical to determine the torsional and inversion barriers to quantify the splittings over the energy levels⁵⁹.

In this work, the torsional potential surface of the large-amplitude motion of the methyl top of the C1 conformer has been calculated with respect to the dihedral angle H4C1N5H6 at the MP2/aug-cc-PVTZ level of theory. It has been computed by fixing the angle C7N5H6 at equilibrium, allowing for the free rotation of the methyl internal rotor. The resulting torsional potential, shown in Fig. 5, yields a barrier height of approximately 631 cm⁻¹. The only experimental estimate available for this parameter, 262 cm⁻¹ was obtained through an experimental procedure¹⁶, and is significantly lower than the present theoretical value. This discrepancy is also evident when compared with the torsional barrier 1322 cm⁻¹ from CH₃NHCl, which share a similar molecular framework. The experimental value showed better agreement with molecular structures, such as CH₃–N=N⁺=N⁻ with a barrier of 250 cm⁻¹. Further experimental and theoretical investigations are therefore warranted to establish a more accurate determination of this barrier.

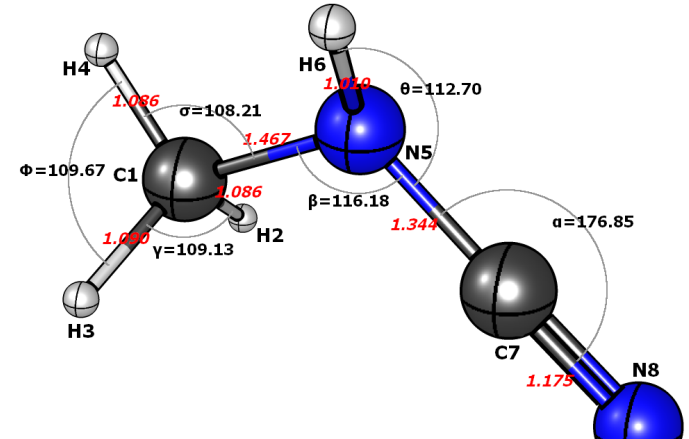


Figure 4. Optimised equilibrium geometry of MCA (bond lengths (in Å, red) and bond angles (in degrees, black)) calculated using CCSD(T)-F12/cc-pVTZ-F12

D. Reaction Pathways

In this section, before addressing the calculation of the reaction pathways, we compute the excitation energies, the linestrengths and the dipole moments of the isomers A1, A2, A3, C1, C2 and C3 using the Single Excitation Configura-

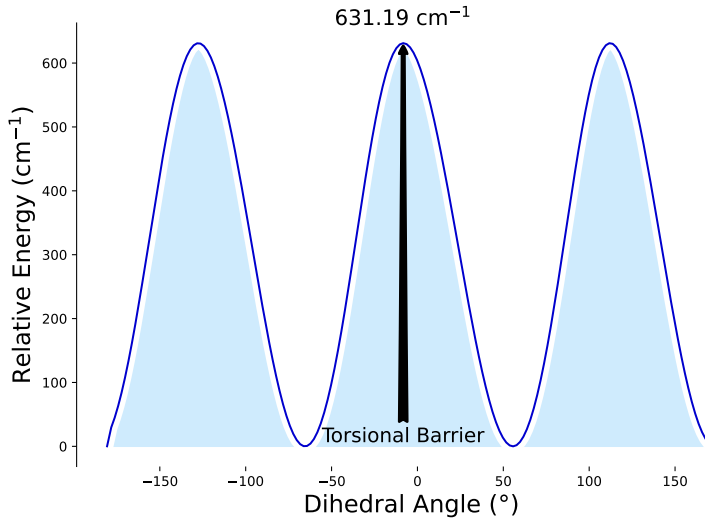


Figure 5. Torsional potential energy surface of CH_3 top of the species MCA computed at the MP2/aug-cc-PVTZ level of theory with respect to the dihedral angle H4C1N5H6.

tion Interaction (CIS). Figure 6 shows a simplified comparison of the trends of the electronic excitation energies, in eV and wavelength, for the isomers A1-A3, and C1-C3, providing insights on their absorption behaviour. Based on the table 9, it can be noted in Fig. 6 that the lowest excited electronic states, at the bottom-left, belong to A3, A2, C3 whereas the highest excited state, at the top-right, is from C1. Table 9 reports the calculated excitation energies, wavelengths and oscillator strengths of the first three excited states of A1, A2, A3, and C1, C2 and C3 isomers. It can be highlighted that isomers A2, C3 and A3 present the highest intensities of the transitions to the excited state, of which the third excited state of A2 has the highest intensity (0.8495), the third state of C3 has a linestrength of 0.7883 and the third state of A3 has an intensity of 0.2718. Table 9 also shows the third electronic states of C3, A2 and A3 have the highest dipole moments with values of 2.9650 au, 2.1702 au and 1.2932 au, respectively. In particular, for the first three excited states of C1, C2 and C3 isomers, the energies of the first three excited states of C1 are computed as 6.48, 7.16, and 7.70 eV, for C2 they are 6.94, 7.11, and 7.31 eV, and for C3 they are 5.39, 6.27, and 7.23 eV. All these excited states absorb photons in the UV region, with wavelengths less than 230 nm, corresponding with the vacuum ultraviolet (VUV) absorption whose wavelengths $< 200 \text{ nm}^{60}$. These underscore possible photochemical dissociation forming reactive species that can recombine or contribute to complex chemical reaction networks via the absorption of vacuum ultraviolet (VUV) in the ISM or in planetary atmospheres⁶¹. The intensities are weaker for the first two excited states of all isomers. However, the third electronic transition of A2, A3, and C3 have relatively high linestrengths. In addition, as the first excited state of A3 is 5.3589 eV, C3 is at 5.3949 eV, while A2 is 5.5304 eV, A3 has higher probability of absorbing photon at that energy with oscillator strength of 0.0027. It is

expected that A2, A3 and C3 are top candidate that are most likely UV-photochemically active species in the first and third excited states amongst the 6 isomers.

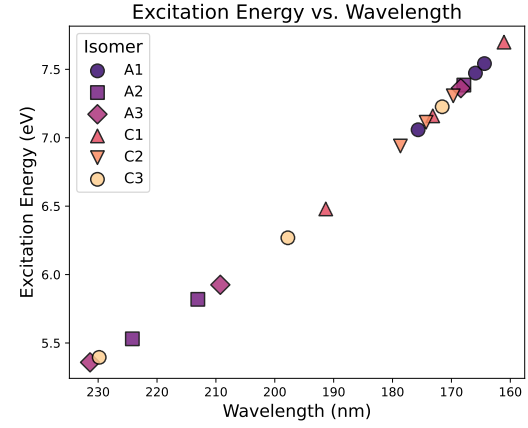


Figure 6. Illustration of trends in the electronic excitations between the first row isomers (A1-A3 and C1-C3)

Table 9. Determination of excitation energies of the first row isomers (A1, A2, A3, C1, C2, and C3) of $\text{C}_2\text{H}_4\text{N}_2$ computed using configuration interaction singles (CIS)

Isomer	Excited State	Elec. state	Excita. Energy (eV)	Wave length (nm)	Oscillator Strength	Dipole Strength (au)
A1	1	$^1\text{A}''$	7.0583	175.66	0.0001	0.0003
	2	$^1\text{A}'$	7.4726	165.92	0.0106	0.0578
	3	$^1\text{A}''$	7.5419	164.39	0.0007	0.0035
A2	1	$^1\text{A}_u$	5.5304	224.19	0.0027	0.0200
	2	$^1\text{B}_g$	5.8190	213.07	0.0000	0.0000
	3	$^1\text{B}_u$	7.3850	167.89	0.8652	4.7819
A3	1	$^1\text{A}''$	5.3586	231.37	0.0007	0.0056
	2	$^1\text{A}''$	5.9253	209.25	0.0078	0.0539
	3	$^1\text{A}'$	7.3625	168.40	0.8495	4.7096
C1 (MCA)	1	^1A	6.4797	191.34	0.0004	0.0023
	2	^1A	7.1598	173.17	0.0036	0.0206
	3	^1A	7.6986	161.05	0.0021	0.0113
C2	1	^1A	6.9398	178.66	0.0003	0.0020
	2	^1A	7.1135	174.29	0.0003	0.0739
	3	^1A	7.3065	169.69	0.0092	0.0511
C3	1	$^1\text{A}''$	5.3949	229.82	0.0003	0.0023
	2	$^1\text{A}''$	6.2688	197.78	0.0029	0.0188
	3	$^1\text{A}'$	7.2263	171.57	0.7883	2.9650

Next, we studied the formation and dissociation pathways using the intrinsic reaction coordinate (IRC). We have ensured that every transition state is a first-order saddle point, whose reaction coordinate ρ is characterised by

$$\frac{\partial^2 W}{\partial \rho^2} \begin{cases} < 0, & \text{for transition states} \\ > 0, & \text{for all other points (initial and final)} \end{cases} \quad (4)$$

where W is the potential energy³⁷. The forward reactions were characterised by a positive transition vector components

whereas the backward reactions were characterised by negative transition vector components in the direction of the reaction coordinate.

Table 10 shows the reaction paths leading to the formation and destruction of MCA and some of the other isomers of the $C_2H_4N_2$ including their activation energies and enthalpies. Table 10 presents the possible reactions involving the species MCA(C1), C2, and C3, as well as A2 and A3, and are organized according to them. Most of the studied reaction pathways are illustrated in Figs. 7 and 8. Out of these reactions we constructed Fig. 8 with reference to CH_3NHCN . In Figure 8, R_n refers to the reaction number, T_n designates the corresponding transition state, and the products of reaction are denoted by Pd_n for the associated reaction. The reactions follow a pathway from reactant(s) (minima) through transition states (TS n , where n is the reaction number) to products. The activation energy (E_a) for all the reactions studied here were computed.

In reaction R1— CH_3NHCN is formed via the neutral-neutral addition of molecular hydrogen (H_2) to $CHNHCN$. The transition state (TS), with an activation energy of 49.40 kJ mol^{-1} , is characterised by an elongated N—H bond and an emerging H—H distance. This indicates a concerted hydrogen abstraction in which one hydrogen atom, initially bonded to a nitrogen center, migrates toward a second hydrogen atom nearby, forming a transient dihydrogen (H_2) moiety. This is a significant process, as neutral-neutral reactions contribute to the formation of COMs, especially in the ISM⁶³.

Reaction R2, there was an electrostatic attraction between molecular hydrogen (H_2) and Nitrogen of CH_2NHCN and the other hydrogen atom with carbon of $-CH_2$ -moeity of CH_2NHCN . The process led to the formation of a transition state with a high activation energy ($205.50\text{ kJ mol}^{-1}$) then followed by elongation of the hydrogen molecule and bringing about a homolytic cleavage, hydrogen transfer then lead to stabilisation and formation of CH_3NHCN . Similar or different processes can be seen for other reactions such as R3; atoms rearrangement followed by proton transfer and subsequent N—C bond cleavage to yield the dissociation products etc. Some of these transition states through each reaction is shown in figure 8. The plot showcases formation/destruction pathways of C1 that are related by species that have been detected in the ISM, for example, CH_2NHCN in R2 pathway ($CH_2NHCN + H_2 \rightarrow CH_3NHCN$) has been detected in the Galactic Center molecular cloud G+0.693-0.027⁶⁴. The reactant in R1 corresponding to $CHNHCN$ is an isomer of CH_2NHCN and H_2 is an abundant specie in the universe and detected in the ISM⁶⁵, and R3 and R14 are connected by dissociation product $HCN + CH_2NH$, both are detected species in different regions such as Sagittarius B2 (Sgr B2)^{66,67}. It also allows the comparison of the relative energies of other reactants and transition states with respect to CH_3NHCN , some of these reactions related to the CH_3NHCN are depicted. The red lines illustrate destruction pathway while the blue lines correspond to the formation pathways.

It is noted that there are some barrierless reactions (the reactions involves radical whose unpaired electrons makes them readily reactive without the need to overcome activation en-

ergy) leading to C1 isomer as a product such as the reactions R6, R10, R12 and R13. The reaction with the highest activation energy corresponds to reaction R3 and R14 with R3 being $429.35\text{ kJ mol}^{-1}$ at coupled-Cluster level of theory while R14 has $386.04\text{ kJ mol}^{-1}$ at CCSD(T)/aug-cc-pVTZ. CH_2NH and HCN are species commonly encountered during the formation and dissociation of CH_3NHCN as indicated by the forward and reverse reactions R3 and R14 passes through different transition states as illustrated in Figure 8, while R3 is an endothermic dissociation pathway , R14 is a exothermic formation pathway. However, the large activation energy in both reactions is not typical in the ISM. Therefore, such reactions would require energetic process (e.g., UV irradiation, cosmic rays) or catalytic surfaces. In terms of the enthalpy of the reactions, exothermic reactions are R1, R2, R4, R7, R9, R11, R14 for C1; R15 and R16 for C2; R19 and R20 for C3; and R22 for A2. It is worthy to note that most of these exothermic reactions are formation pathways whereas the endothermic reactions involving C1 species are those numbered as R3, R5, and R8; R18 involving C3; and R21 for A3. Reaction R5 is a decomposition reaction of cyanodimethylamine yielding MCA and methylene. This reaction, which occurs via a hydrogen shift to the amine nitrogen followed by cleavage of the $-CH_2$ group, is characterised by an endothermic enthalpy CCSD(T)/aug-cc-pVTZ energy barrier of $423.75\text{ kJ mol}^{-1}$ (1.74 eV)). According to the spin selection rules for allowed and forbidden reactions⁶⁸, which forbid transitions between states with different total spin and different spin multiplicity, all reactants involved in the formation of MCA (first section of Table 10) occur in the singlet state ($^1\Sigma$), similarly to the product (MCA). In summary, it can be inferred from our analysis that several reaction generating MCA, as well as species C2, C3, A2 and A3, are potentially feasible.

E. Atmospheric and Astrophysical implications

The detection of several key reactants —such as methanimine (CH_2NH), hydrogen cyanide (HCN), and the hydroxyl radical (OH)^{69–71}— in various layers of Earth’s atmosphere supports the current hypotheses regarding the atmospheric roles of the molecular species studied in Table 10. For example, the dissociation products in reaction R3 are methanimine (CH_2NH) and hydrogen cyanide (HCN). Methylene imine (CH_2NH) has been found in the ionospheric layer of the Earth’s atmosphere⁶⁹ whereas HCN is found in both the troposphere and stratosphere of the Earth⁷². This implies that, if present in the atmosphere, MCA would undergo decomposition to methylene imine and HCN . HCN is a known toxic compound found in different parts of the atmosphere⁷². Reaction R5 shows MCA can also be obtained from the decomposition of dimethylcyanamide ($(CH_3)_2NHCN$) into MCA and methylene CH_2 , which is a highly reactive intermediate and a part of many compounds such as drugs, fossil fuels and plastics via its ability to act as an adduct⁷³. CH_2 is present in methane-oxygen and ethylene-oxygen flames⁷⁴. Reactions R1 and R9, with low activation energies relatively close to the thermal energy available in the atmosphere ($\sim 3.7\text{ kJ/mol}$),

Table 10. Formation and destruction pathways of CH_3NHCN provided with their activation energies and enthalpies (in kJmol^{-1} and eV) computed at B3LYP/6-31g(d,p)//CCSD(T)/aug-cc-pVTZ levels

Reaction Number	Reaction	Type	Activation energy kJ mol^{-1} (eV)	Enthalpy of reaction kJ mol^{-1} (eV)	Overall reaction
R1	$\text{CHNHCN} + \text{H}_2 \rightarrow \text{CH}_3\text{NHCN}$	Form.	49.40 (0.51)	-365.57 (-3.78)	Exo
R2	$\text{CH}_2\text{NCN} + \text{H}_2 \rightarrow \text{CH}_3\text{NHCN}$	Form.	205.50 (2.13)	-300 (-3.11)	Exo.
R3	$\text{CH}_3\text{NHCN} \rightarrow \text{CH}_2\text{NH} + \text{HCN}$	Dest.	430.12 (4.45)	84.47 (0.87)	Endo.
R4	$\text{CH}_3\text{NHCN} \rightarrow \text{CH}_2\text{NH}_2\text{CN}$	Dest.	387.87 (4.02)	-341.83 (-3.54)	Exo.
R5	$(\text{CH}_3)_2\text{NHCN} \rightarrow \text{CH}_3\text{NHCN} + \text{CH}_2$	Form.	350.24 (3.63)	423.75 (4.39)	Endo.
R6	$\text{CH}_3\text{NH} + \text{CN} \rightarrow \text{CH}_3\text{NHCN}$	Form.	0.0		Barrierless
R7	$\text{CH}_3\text{NHCN} + \text{H}_2 \rightarrow \text{CH}_3\text{NH}_2 + \text{HCN}$	Dest.	335.76 (3.48)	-28.61 (-0.29)	Exo.
R8	$\text{CH}_3\text{NHCN} \rightarrow \text{CH}_3\text{NCNH}$	Dest.	347.34 (3.60)	80.32 (0.83)	Endo.
R9	$\text{CH}_3\text{NHCN} + \text{H} \rightarrow \text{CH}_3\text{NHCNH}$	Dest.	31.84 (0.33)	-100.90 (-1.04)	Exo.
R10	$\text{OH} + \text{CH}_3\text{NH}_2\text{CN} \rightarrow \text{CH}_3\text{NHCN} + \text{H}_2\text{O}$	Form.	0.0 (0.0)		Barrierless
R11	$\text{OH} + \text{CH}_3\text{NHCNH} \rightarrow \text{CH}_3\text{NHCN} + \text{H}_2\text{O}$	Form.	260.47 (2.69)	-44.64 (-0.462)	Exo.
R12	$\text{CH}_3\text{NCN} + \text{H} \rightarrow \text{CH}_3\text{NHCN}$	Form.	0.0		Barrierless
R13	$\text{CH}_3 + \text{HNCN} \rightarrow \text{CH}_3\text{NHCN}$	Form.	0.0		Barrierless
R14	$\text{CH}_2\text{NH} + \text{HCN} \rightarrow \text{CH}_3\text{NHCN}$	Form.	386.04 (4.00)	-84.47 (-0.87)	Exo.
R15	$\text{H}_2 + \text{HCNCNH} \rightarrow \text{CH}_3\text{NCNH}$	Form.	45.63 (0.47)	-232.03 (-2.40)	Exo.
R16	$\text{CH}_2\text{NCHNH} \rightarrow \text{CH}_3\text{NCNH}$	Form.	322.97 (3.34)	-16.72 (0.17)	Exo.
R17	$\text{CH}_3\text{NCN} + \text{H} \rightarrow \text{CH}_3\text{NCNH}$	Form.	0.0		Barrierless
R18	$\text{CH}_2\text{NCHNH} \rightarrow \text{HNC} + \text{CH}_2\text{NH}$	Dest.	320.02 (3.31)	93.66 (0.97)	Endo.
R19	$\text{CH}_2\text{NCN} + \text{H}_2 \rightarrow \text{CH}_2\text{NCHNH}$	Form.	319.75 (3.31)	-103.46 (-1.07)	Exo.
R20	$\text{HCN} + \text{HNC} + \text{H}_2 \rightarrow \text{CH}_2\text{NCHNH}$	Form.	153.20 (1.58)	-192.26 (-1.99)	Exo.
R21	$\text{cis-NHCCHCHNH} \rightarrow \text{CHNH}_2^+ + \text{HCN}$	Dest.	208.61 (2.16)	200.41 (2.38)	Endo.
R22	$\text{NH}_2\text{CCHNH} \rightarrow \text{trans-NHCCHCHNH}$	Form.	219.68 (2.27)	-155.10 (-1.61)	Exo

Based on benchmarking of the chosen *ab initio* methods, an uncertainty of 3.0–4.5 kJ mol^{-1} at the CCSD(T)/aug-cc-pVTZ level of theory⁶² can be expected. Barrier heights for formation and dissociation of CH_3NHCN (C1) from R1 to R14; CH_3NCNH (C2), from R15 to R17; and CH_2NCHNH (C3), from R18 to R20. 1,2-di-iminoethane or NHCHCHNH represented by R21 and R22, respectively.

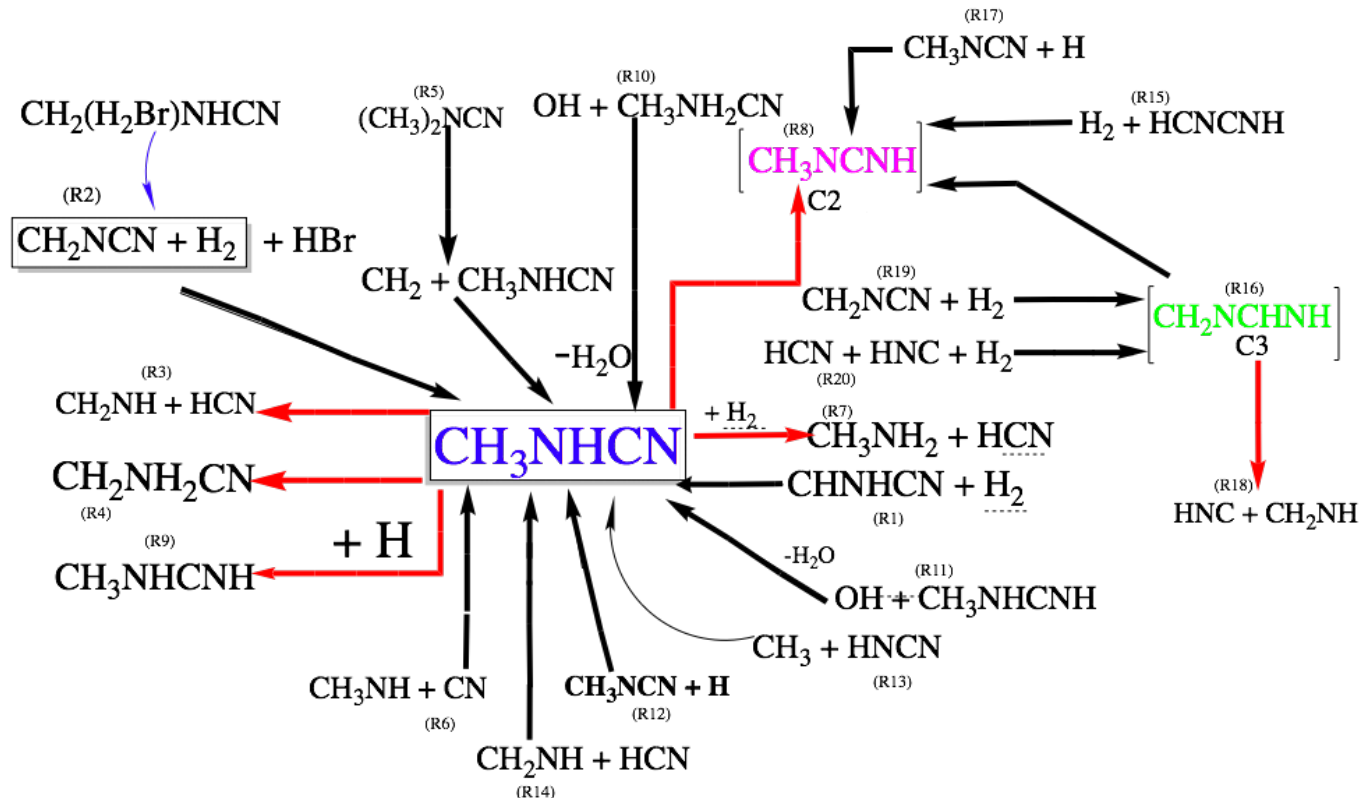


Figure 7. Gas-phase reaction network for the formation and destruction of MCA, C2 and C3. Each reaction is numbered, formation pathways are depicted by black arrows, destruction and pathways leading to other products are depicted by red arrows whereas intermediate path is shown with a blue arrow.

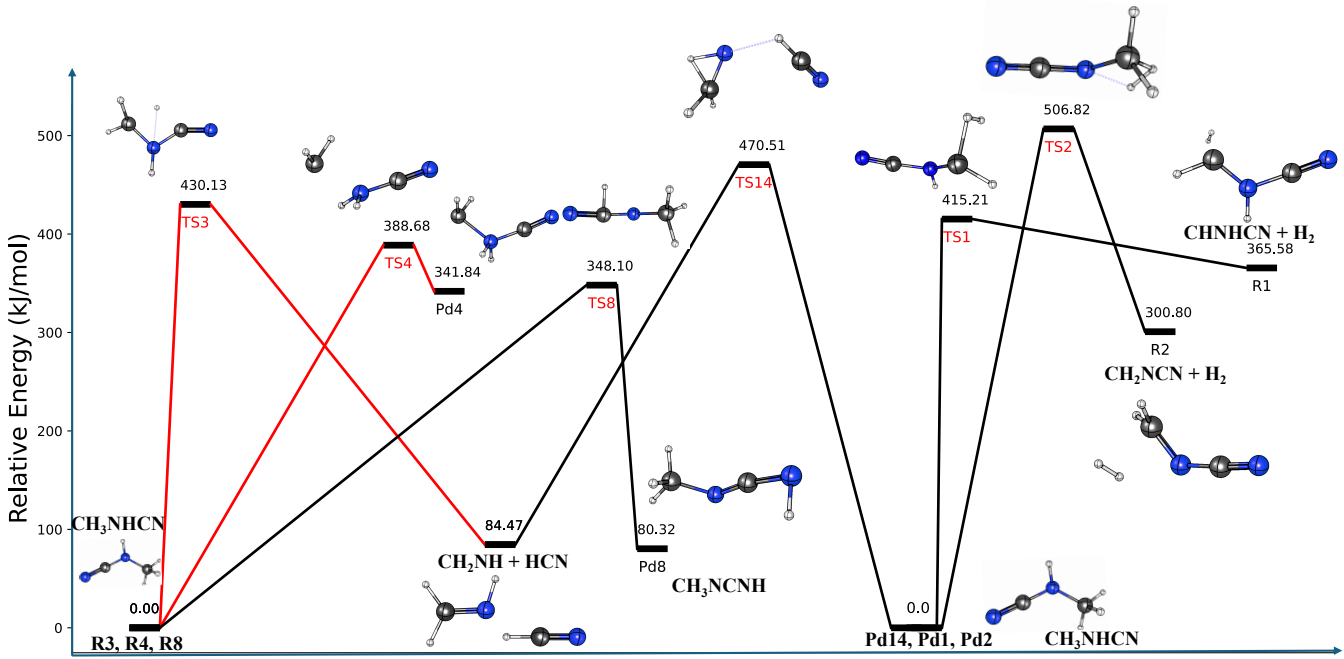


Figure 8. Some studied reaction pathways of formation and destruction of MCA computed at the B3LYP/6-31g(d,p)//CCSD(T)/aug-cc-pVTZ, where black lines corresponds to formation pathways and red lines corresponds to destruction pathways.

could be expected feasible in the lower layers of the atmosphere. The exothermic reaction R7, from MCA, gives methylamine (CH₃NH₂) as product, which is detected in the atmosphere⁷⁵ and could be present in the upper atmosphere of Titan, reacting with CN radicals to form MCA and other N-bearing organic compounds⁵⁰. In addition, there are four barrierless reactions R6, R10, R12 and R13 forming the conformer C1 as well as another formation reaction R17 of conformer C2.

In astrophysical environments, N-bearing molecules are among the most abundant species in sources such as the Taurus Molecular Cloud (TMC-1)⁷. The new finding of N-bearing molecules in star-forming regions, protoplanetary disks, and other interstellar sources is relevant for paving the way for the astrochemical understanding and modeling of the reaction mechanisms in dust-grains and in the gas phase processes⁷⁶. It is expected that, apart from the barrierless reactions, the other reactions studied in Table 10 could also occur in the ISM sources. For instance, the reaction R1 coming from the association between CHNHCN and hydrogen radicals has a low activation energy of 0.51 eV. This kind of reactions is relevant in the ISM especially in ice-surfaces or dust grains^{65,77}. In reaction R2, two hydrogen radicals add up to the CH₂ and the middle N atom of N-cyanomethanimine (CH₂NCN) forming CH₃NHCN. The compound CH₂NCN has been already detected in space⁶⁴ and its isomer CHNHCN in reaction R1 can be formed by tautomeric transfer of a hydrogen from the carbon atom to the nitrogen atom.

MCA (CH₃NHCN) dissociates into (CH₂NH) and the HCN in reaction R3, which products have been identified in ISM sources^{63,66,78} as well as CH₂NH is known to play a vital role in prebiotic chemistry and the formation of amino acid⁷⁹. Reaction R4 is basically an isomerisation reaction between CH₃NHCN to CH₂NH₂CN, involving a transfer of one hydrogen atom from the methyl group (CH₃) to NH group. In addition, the reactions with high barrier heights in Table 10 could also occur in moderately high kinetic temperatures environments, such as Galactic center molecular clouds, or in regions with higher energy processes, radiation and/or shock fronts, provided that there is an additional energy source, like UV radiation or catalyst, i.e., the reaction could be triggered at any environment when there are appropriate chemical and physical conditions⁸⁰.

The present results provide new pathways and thermochemical data for N-bearing reactions for which no previous formation pathways or barrier information was available. These reactions, particularly those involving CH₂NH, CH₃NH, and HCN derivatives, are relevant to the formation of methylcyanamide (MCA) and other related species, which have been proposed as precursors of interstellar glycine. The calculated reaction enthalpies and activation energies can be incorporated into astrochemical reaction networks such as UMIST⁸¹ and KIDA⁸² to improve the modeling of nitrogen chemistry in hotcores, dense molecular clouds, and protoplanetary disks. Inclusion of these pathways/thermochemical parameters will refine gas-gas or gas-grain code for abundance

estimation^{83,84} enhance the predictive capacity of interstellar chemical models. MCA (CH_3NHCN) and other conformers A1, A2, A3, C2 and C3 have absorption wavelengths within the range critical for photochemistry (115–230 nm) (see Tab. 9). Thus, they can be involved in photochemical reactions of interest to determine the composition of gas giant exoplanetary atmospheres⁶⁰. The James Webb Space Telescope (JWST) observed the evidence of photochemistry and its impact in the atmospheres of exoplanets like the gas giant WASP-39b⁸⁵.

Besides, the thermal dependence of VUV absorption cross sections of molecules are not well known at the characteristic temperatures of the observed exoplanet atmospheres⁶⁰ and, therefore, this study can also hint at the photochemical processes of these molecules on them. Most of the reactions in Table 10 have high activation energies but below the excitation energies of the conformers A1-A3 and C1-C3 provided in Table 9. Consequently, it could be expected that a combination of the photochemistry processes and the reactions studied here could produce the conformers of $\text{C}_2\text{H}_4\text{N}_2$ and other molecular species key in the exoplanetary atmospheres.

IV. CONCLUSIONS

This comprehensive study of the family of isomers $\text{C}_2\text{H}_4\text{N}_2$ includes the *ab initio* calculation of their electronic ground state and excitation energies, structural geometries, spectroscopic rotational and vibrational parameters, dipole moments, and the activation energies and enthalpies in some reaction pathways involving conformers C1, C2 and C3. The electronic energies for all the conformers have been computed using the high level CCSD(T)-F12/cc-pVTZ-F12 and spectroscopic parameters using correlated *ab initio* methods CCSD(T)/cc-pVTZ and MP2/aug-cc-pVTZ. These have shown a good agreement with the available experimental and computed data. The dipole moments of the isomers A1-A4 and C1-C4 have been computed with significant values larger than 2 D. In particular, the conformer methylcyanamide (C1 or MCA) has a notable large dipole moment of 5.04 D in comparison to other isomers of the family and is the next most energetically stable species lying at 0.27 eV (2177.70 cm^{-1}). From these two facts, we would expect plausible its radioastronomical detection.

Excitation energies of the first three isomers of Cn show that C3 has the lowest value of 5.3949 eV compared to 6.4797 eV for MCA and, therefore, it is more reactive than MCA. A study of the chemical network of MCA, C2 and C3 has been carried out to understand the formation and destruction pathways in the gas phase by computing the activation energies and the enthalpies at the level of theory B3LYP/6-31g(d,p)//CCSD(T)/aug-cc-pVTZ. The most probable pathways involve the barrierless processes and other neutral-neutral reactions with relatively low activation energies. The current investigation intends to provide the relevant information for the spectral characterization of the family of isomers $\text{C}_2\text{H}_4\text{N}_2$, of which spectra are incomplete or have never been measured yet. In addition, the calculation of the relevant

quantities for the chemical pathway networks of this set of species will shed light on the abundance evolution patterns in environments such as the Earth's atmosphere and ISM after incorporating them into the atmospheric or astrochemical models.

V. SUPPLEMENTARY MATERIAL

The supplementary material provides information on the remaining isomers that are not included in the main text. It includes three sections: The first section describes the relevant structural parameters of isomers with higher electronic energy; The second section presents the harmonic and anharmonic vibrational frequencies of isomers with higher electronic energy; and the third section reports the rotational and centrifugal distortion constants of the isomers.

ACKNOWLEDGMENTS

This work was supported by a PhD scholarship from the DCA, Universidad Autónoma de Chile. NI acknowledges FONDECYT grant N°1241193 and VRIP. This project has also received funding from the European Union's Horizon 2020 research and innovation program under Marie Skłodowska-Curie grant agreement No. 872081, and grant PID2022-136228NB-C21 (M.C.) funded by MCIN/AEI/10.13039/501100011033, and, as appropriate, by "ERDF A way of making Europe", the "European Union", or the "European Union NextGenerationEU/PRTR". This work is also supported by the Consejería de Transformación Económica, Industria, Conocimiento y Universidades, Junta de Andalucía and European Regional Development Fund (ERDF 2021-2027) under the project EPIT1462023 (M.C. and E.M.).

REFERENCES

- ¹M. A. Ali and S. R., *Scientific Reports* **14** (2024), 10.1038/s41598-024-70721-y.
- ²V. P. Kanawade and colleagues, *Communications Earth & Environment* **6**, 38 (2025).
- ³C. J. Nielsen, H. Herrmann, and C. Weller, *Chemical Society Reviews* **41**, 6684 (2012).
- ⁴J. N. Galloway, J. D. Aber, J. W. Erisman, S. P. Seitzinger, R. W. Howarth, E. B. Cowling, and B. J. Cosby, *Bioscience* **53**, 341 (2003).
- ⁵T. Suzuki, M. Ohishi, M. Saito, T. Hirota, L. Majumdar, and V. Wakelam, *Astrophys. J. Suppl. Ser.* **237**, 3 (2018).
- ⁶V. T. Rezende, T. Bonaudo, R. B. Alves, R. A. Nascimento, and A. H. Gameiro, *Nitrogen* **2**, 128 (2021).
- ⁷L.-F. Chen, D. Li, D. Quan, X. Zhang, Q. Chang, X. Li, and L. Xiao, *The Astrophysical Journal* **928**, 175 (2022).
- ⁸M. Carvajal, C. Favre, I. Kleiner, C. Ceccarelli, E. A. Bergin, and D. Fedele, *Astronomy & Astrophysics* **627**, A65 (2019).
- ⁹E. Bogelund, B. McGuire, M. Hogerheijde, E. van Dishoeck, and N. Ligerink, *A&A* **624**, A82 (2019).
- ¹⁰C. M. Canelo, L. Bronfman, E. Mendoza, N. Duronea, M. Merello, M. Carvajal, A. C. S. Friaça, and J. Lepine, *Monthly Notices of the Royal Astronomical Society* **504**, 4428 (2021).

¹¹K.-J. Chuang, C. Jäger, S. A. Krasnokutski, D. Fulvio, and T. Henning, *The Astrophysical Journal* **933**, 107 (2022).

¹²M. Carvajal, C. Favre, I. Kleiner, C. Ceccarelli, E. A. Bergin, and D. Fedele, *Astronomy & Astrophysics* **685**, C1 (2024).

¹³J. C. Ramal-Olmedo, C. A. Menor-Salván, A. Miyoshi, and R. C. Fortenberry, *Astronomy & Astrophysics* **672**, A49 (2023).

¹⁴M. Melosso, A. Belloche, M.-A. Martin-Drumel, O. Pirali, F. Tamassia, L. Bizzocchi, R. T. Garrod, H. S. P. Müller, K. M. Menten, L. Dore, and C. Puzzarini, *Astronomy & Astrophysics* **641**, A160 (2020).

¹⁵A. Manna and S. Pal, *Life Sciences in Space Research* **34**, 9 (2022).

¹⁶B. Bak and H. Svanholt, *Acta Chemica Scandinavica A* **34**, 57 (1980).

¹⁷N. Inostroza-Pino, C. Z. Palmer, T. J. Lee, and R. C. Fortenberry, *Journal of Molecular Spectroscopy* **369**, 111273 (2020).

¹⁸M. McKissick and R. C. Fortenberry, *ACS Earth and Space Chemistry* **9**, 403–410 (2025).

¹⁹K. Nair, J. Demaison, G. Wlodarczak, and I. Merke, *Journal of Molecular Spectroscopy* **237**, 137 (2006).

²⁰N. Inostroza and M. Senent, *Chemical Physics Letters* **524**, 25 (2012).

²¹M. McCarthy and K. L. K. Lee, *The Journal of Physical Chemistry A* **124**, 3002 (2020).

²²M. L. Senent, M. Hochlaf, and M. Carvajal, *The Journal of Physical Chemistry A* **120**, 475 (2016).

²³T. B. Adler, G. Knizia, and H.-J. Werner, *J. Chem. Phys.* **127**, 221106 (2007).

²⁴G. Knizia, T. B. Adler, and H.-J. Werner, *J. Chem. Phys.* **130**, 054104 (2009).

²⁵H.-J. Werner, P. J. Knowles, G. Knizia, F. R. Manby, M. Schütz, P. Celani, W. Györffy, D. Kats, T. Korona, R. Lindh, A. Mitrushenkov, G. Rauhut, K. R. Shamasundar, T. B. Adler, R. D. Amos, A. Bernhardsson, A. Berning, D. L. Cooper, M. J. O. Deegan, A. J. Dobbyn, F. Eckert, E. Goll, C. Hampel, A. Hesselmann, G. Hetzer, T. Hrenar, G. Jansen, C. Köpli, Y. Liu, A. W. Lloyd, R. A. Mata, A. J. May, S. J. McNicholas, W. Meyer, M. E. Mura, A. Nicklass, D. P. O'Neill, P. Palmieri, D. Peng, K. Pflüger, R. Pitzer, M. Reiher, T. Shiozaki, H. Stoll, A. J. Stone, R. Tarroni, T. Thorsteinsson, and M. Wang, “MOLPRO, version 2015.1, a package of ab initio programs,” (2015), see <http://www.molpro.net>.

²⁶T. B. Adler, G. Knizia, and H.-J. Werner, *Journal of Chemical Physics* **127**, 221106 (2007).

²⁷T. H. D. Jr., *Journal of Chemical Physics* **90**, 1007 (1989).

²⁸H. Kruse, R. Szabla, and J. Šponer, *The Journal of Chemical Physics* **152** (2020), 10.1063/5.0006871.

²⁹C. Møller and M. S. Plesset, *Physical Review* **46**, 618–622 (1934).

³⁰K. Raghavachari, G. W. Trucks, J. A. Pople, and M. Head-Gordon, *Chemical Physics Letters* **157**, 479 (1989).

³¹M. J. Frisch, G. W. Trucks, H. B. Schlegel, G. E. Scuseria, M. A. Robb, J. R. Cheeseman, G. Scalmani, V. Barone, B. Mennucci, G. A. Petersson, H. Nakatsuji, M. Caricato, X. Li, H. P. Hratchian, A. F. Izmaylov, J. Bloino, G. Zheng, J. L. Sonnenberg, M. Hada, M. Ehara, K. Toyota, R. Fukuda, J. Hasegawa, M. Ishida, T. Nakajima, Y. Honda, O. Kitao, H. Nakai, T. Vreven, J. A. Montgomery, Jr., J. E. Peralta, F. Ogliaro, M. Bearpark, J. J. Heyd, E. Brothers, K. N. Kudin, V. N. Staroverov, R. Kobayashi, J. Normand, K. Raghavachari, A. Rendell, J. C. Burant, S. S. Iyengar, J. Tomasi, M. Cossi, N. Rega, J. M. Millam, M. Klene, J. E. Knox, J. B. Cross, V. Bakken, C. Adamo, J. Jaramillo, R. Gomperts, R. E. Stratmann, O. Yazyev, A. J. Austin, R. Cammi, C. Pomelli, J. W. Ochterski, R. L. Martin, K. Morokuma, V. G. Zakrzewski, G. A. Voth, P. Salvador, J. J. Dannenberg, S. Dapprich, A. D. Daniels, A. Farkas, J. B. Foresman, J. V. Ortiz, J. Cioslowski, and D. J. Fox, *Gaussian 09 Revision A.1*, Gaussian Inc., Wallingford, CT (2009), gaussian Inc. Wallingford CT 2009.

³²M. J. Frisch, G. W. Trucks, H. B. Schlegel, G. E. Scuseria, M. A. Robb, J. R. Cheeseman, G. Scalmani, V. Barone, G. A. Petersson, H. Nakatsuji, X. Li, M. Caricato, A. V. Marenich, J. Bloino, B. G. Janesko, R. Gomperts, B. Mennucci, H. P. Hratchian, J. V. Ortiz, A. F. Izmaylov, J. L. Sonnenberg, D. Williams-Young, F. Ding, F. Lippiani, F. Egidi, J. Goings, B. Peng, A. Petrone, T. Henderson, D. Ranasinghe, V. G. Zakrzewski, J. Gao, N. Rega, G. Zheng, W. Liang, M. Hada, M. Ehara, K. Toyota, R. Fukuda, J. Hasegawa, M. Ishida, T. Nakajima, Y. Honda, O. Kitao, H. Nakai, T. Vreven, K. Throssell, J. A. Montgomery, Jr., J. E. Peralta, F. Ogliaro, M. J. Bearpark, J. J. Heyd, E. N. Brothers, K. N. Kudin, V. N. Staroverov, T. A. Keith, R. Kobayashi, J. Normand, K. Raghavachari, A. P. Rendell, J. C. Burant, S. S. Iyengar, J. Tomasi, M. Cossi, J. M. Millam, M. Klene, C. Adamo, R. Cammi, J. W. Ochterski, R. L. Martin, K. Morokuma, O. Farkas, J. B. Foresman, and D. J. Fox, “Gaussian 16, revision C.01,” (2016).

³³O. Yañez, R. Báez-Grez, D. Inostroza, W. A. Rabanal-León, R. Pino-Rios, J. Garza, and W. Tiznado, *Journal of Chemical Theory and Computation* **15**, 1463 (2018).

³⁴Y. Shu, E. G. Hohenstein, and B. G. Levine, *The Journal of Chemical Physics* **142**, 024102 (2015).

³⁵T. H. Dunning, *The Journal of Chemical Physics* **90**, 1007 (1989).

³⁶K. Fukui, *The Journal of Physical Chemistry* **74**, 4161 (1970).

³⁷K. Fukui, *Accounts of Chemical Research* **14**, 363 (1981).

³⁸C. Gonzalez and H. B. Schlegel, *J. Chem. Phys.* **90**, 2154 (1989).

³⁹S. Maeda, Y. Harabuchi, Y. Ono, T. Taketsugu, and K. Morokuma, *International Journal of Quantum Chemistry* **115**, 258 (2014).

⁴⁰J. Tirado-Rives and W. L. Jorgensen, *J. Chem. Theory Comput.* **4**, 297 (2008).

⁴¹I. D. Mackie and G. A. DiLabio, *J. Chem. Phys.* **135**, 134318 (2011).

⁴²M. Villa, M. L. Senent, R. Dominguez-Gomez, O. Alvarez-Bajo, and M. Carvajal, *The Journal of Physical Chemistry A* **115**, 13573–13580 (2011).

⁴³H. M. Pickett, *Journal of Molecular Spectroscopy* **46**, 335–340 (1973).

⁴⁴M. Lattelais, F. Pauzat, Y. Ellinger, and C. Ceccarelli, *The Astrophysical Journal* **696**, L133 (2009).

⁴⁵V. Barone, S. Alessandrini, M. Biczysko, J. R. Cheeseman, D. C. Clary, A. B. McCoy, R. J. DiRisio, F. Neese, M. Melosso, and C. Puzzarini, *Nature Reviews Methods Primers* **1**, 38 (2021).

⁴⁶A. Belloche, K. M. Menten, C. Comito, H. S. P. Müller, P. Schilke, J. Ott, S. Thorwirth, and C. Hieret, *Astronomy & Astrophysics* **482**, 179–196 (2008).

⁴⁷A. D. Bochevarov and C. D. Sherrill, *The Journal of Chemical Physics* **122**, 234110 (2005).

⁴⁸V. I. Minkin, B. Y. Simkin, and R. M. Minyaev, *Feniks*, Rostov-on-Don (1997).

⁴⁹D. P. Tew, in *New Electron Correlation Methods and their Applications, and Use of Atomic Orbitals with Exponential Asymptotes*, Advances in Quantum Chemistry, Vol. 83, edited by M. Musial and P. E. Hoggan (Academic Press, 2021) pp. 83–106.

⁵⁰C. Sleiman, G. El Dib, M. Rosi, D. Skouteris, N. Balucani, and A. Canosa, *Physical Chemistry Chemical Physics* **20**, 5478 (2018).

⁵¹N. Jiang, M. Melosso, S. Alessandrini, L. Bizzocchi, M.-A. Martin-Drumel, O. Pirali, and C. Puzzarini, *Physical Chemistry Chemical Physics* **25**, 4754–4763 (2023).

⁵²I. Toumi, S. Dalbouha, M. M. Al-Mogren, O. Yazidi, N.-E. Jaïdane, M. Carvajal, and M. L. Senent, *The Journal of Physical Chemistry A* **126**, 7230–7241 (2022).

⁵³V. Gámez, M. L. Senent, M. Carvajal, and A. Galano, *The Journal of Physical Chemistry A* **123**, 9658–9668 (2019).

⁵⁴B. Bak, E. L. Hansen, F. M. Nicolaisen, and O. F. Nielsen, *Canadian Journal of Physics* **53**, 2183–2188 (1975).

⁵⁵A. A. Kananenka and J. L. Skinner, *The Journal of Chemical Physics* **148** (2018), 10.1063/1.5037113.

⁵⁶A. K. Eckhardt, *Chemical Communications* **58**, 8484–8487 (2022).

⁵⁷M. L. Senent and S. Dalbouha, *Molecules* **26**, 4269 (2021).

⁵⁸N. Inostroza-Pino, V. Lattanzi, C. Zachary Palmer, R. C. Fortenberry, D. Mardones, P. Caselli, O. E. Godwin, and T. J. Lee, *Mol. Phys.* **122**, e2280762 (2024).

⁵⁹H. El Hadki, V. G. Gámez, S. Dalbouha, K. Marakchi, O. K. Kabbaj, N. Komiha, M. Carvajal, and M. L. Senent Diez, *Open Research Europe* **1**, 116 (2022).

⁶⁰B. Fleury, M. Poveda, Y. Benilan, R. Veillet, O. Venot, P. Tremblin, N. Fray, M.-C. Gazeau, M. Schwell, A. Jolly, N. de Oliveira, and E.-t. Es-sebbar, *Astronomy & Astrophysics* **693**, A82 (2025).

⁶¹Y. Chang, M. N. R. Ashfold, K. Yuan, and X. Yang, *National Science Review* **10** (2023).

⁶²N. A. West, L. H. D. Li, T. J. Millar, M. Van de Sande, E. Rutter, M. A. Blitz, J. H. Lehman, L. Decin, and D. E. Heard, *Physical Chemistry Chemical Physics* **25**, 7719–7733 (2023).

⁶³Mendoza, Edgar, Dall’Olio, Pietro, Coelho, Luciene S., Peregrín, Antonio, López-Domínguez, Samuel, van der Tak, Floris F. S., and Carvajal, Miguel,

A&A **698**, A286 (2025).

⁶⁴D. San Andrés, V. M. Rivilla, L. Colzi, I. Jiménez-Serra, J. Martín-Pintado, A. Megías, Á. López-Gallifa, A. Martínez-Henares, S. Massalkhi, S. Zeng, M. Sanz-Novo, B. Tercero, P. de Vicente, S. Martín, M. A. Requena Torres, G. Molpeceres, and J. García de la Concepción, *Astrophys. J.* **967**, 39 (2024).

⁶⁵V. Wakelam, E. Bron, S. Cazaux, F. Dulieu, C. Gry, P. Guillard, E. Habart, L. Hornecker, S. Morisset, G. Nyman, V. Pirronello, S. D. Price, V. Valdivia, G. Vidali, and N. Watanabe, *Molecular Astrophysics* **9**, 1–36 (2017).

⁶⁶M. D. Gorski, S. Aalto, J. Mangum, E. Momjian, J. H. Black, N. Falstad, B. Gullberg, S. König, K. Onishi, M. Sato, and F. Stanley, *Astronomy & Astrophysics* **654**, A110 (2021).

⁶⁷L. Neumann, F. Bigiel, A. T. Barnes, M. J. Gallagher, A. Leroy, A. Usero, E. Rosolowsky, I. Bešlić, M. Boquien, Y. Cao, M. Chevance, D. Colombo, D. A. Dale, C. Eibensteiner, K. Grasha, J. D. Henshaw, M. J. Jiménez-Donaire, S. Meidt, S. H. Menon, E. J. Murphy, H.-A. Pan, M. Querejeta, T. Saito, E. Schinnerer, S. K. Stuber, Y.-H. Teng, and T. G. Williams, *Astronomy & Astrophysics* **691**, A121 (2024).

⁶⁸J. N. Harvey, *Phys. Chem. Chem. Phys.* **9**, 331 (2007).

⁶⁹B. Fleury, L. Vettier, and N. Carrasco, *EPSC Abstracts* **10**, EPSC2015 (2015).

⁷⁰A. G. Bruno, J. J. Harrison, M. P. Chipperfield, D. P. Moore, R. J. Pope, C. Wilson, E. Mahieu, and J. Notholt, *Atmospheric Chemistry and Physics* **23**, 4849–4861 (2023).

⁷¹D. E. Heard, *Annual Review of Physical Chemistry* **57**, 191–216 (2006).

⁷²R. J. Cicerone and R. Zellner, *Journal of Geophysical Research: Oceans* **88**, 10689 (1983).

⁷³I. Shavitt, *Tetrahedron* **41**, 1531 (1985).

⁷⁴J. Peeters and C. Vinckier, *Symposium (International) on Combustion* **15**, 969 (1975).

⁷⁵F. Yu and G. Luo, *Atmospheric Chemistry and Physics* **14**, 12455 (2014).

⁷⁶S. K. Mondal, W. Iqbal, P. Gorai, B. Bhat, V. Wakelam, and A. Das, *Astronomy & Astrophysics* **669**, A71 (2023).

⁷⁷W. Cui and E. Herbst, *ACS Earth and Space Chemistry* **8**, 2218–2231 (2024).

⁷⁸J. E. Dickens, W. M. Irvine, C. H. DeVries, and M. Ohishi, *The Astrophysical Journal* **479**, 307–312 (1997).

⁷⁹C. Zhu, R. Frigge, A. M. Turner, M. J. Abplanalp, B.-J. Sun, Y.-L. Chen, A. H. H. Chang, and R. I. Kaiser, *Physical Chemistry Chemical Physics* **21**, 1952 (2019).

⁸⁰N. Inostroza-Pino, O. Emmanuel Godwin, D. Mardones, and J. Ge, *Astron. Astrophys.* **688**, A140 (2024).

⁸¹T. J. M. et al., *Astronomy and Astrophysics* (2023), available online: <https://umistdatabase.uk/>.

⁸²V. Wakelam, P. Gratier, J.-C. Loison, K. M. Hickson, J. Penguen, and A. Mechineau, *Astronomy & Astrophysics* **689**, A63 (2024).

⁸³W. Iqbal and V. Wakelam, *Astronomy & Astrophysics* **615**, A20 (2018).

⁸⁴J. Ge, *Research in Astronomy and Astrophysics* **22**, 015004 (2022).

⁸⁵S.-M. Tsai, E. K. H. Lee, D. Powell, P. Gao, X. Zhang, J. Moses, E. Hébrard, O. Venot, V. Parmentier, S. Jordan, R. Hu, M. K. Alam, L. Alderson, N. M. Batalha, J. L. Bean, B. Benneke, C. J. Bierson, R. P. Brady, L. Carone, A. L. Carter, K. L. Chubb, J. Inglis, J. Leconte, M. Line, M. López-Morales, Y. Miguel, K. Molaverdikhani, Z. Rustamkulov, D. K. Sing, K. B. Stevenson, H. R. Wakeford, J. Yang, K. Aggarwal, R. Baeyens, S. Barat, M. de Val-Borro, T. Daylan, J. J. Fortney, K. France, J. M. Goyal, D. Grant, J. Kirk, L. Kreidberg, A. Louca, S. E. Moran, S. Mukherjee, E. Nasedkin, K. Ohno, B. V. Rackham, S. Redfield, J. Taylor, P. Tremblin, C. Visscher, N. L. Wallack, L. Welbanks, A. Youngblood, E.-M. Ahrer, N. E. Batalha, P. Behr, Z. K. Berta-Thompson, J. Blecic, S. L. Casewell, I. J. M. Crossfield, N. Crouzet, P. E. Cubillos, L. Decin, J.-M. Désert, A. D. Feinstein, N. P. Gibson, J. Harrington, K. Heng, T. Henning, E. M.-R. Kempton, J. Krick, P.-O. Lagage, M. Lendl, J. D. Lothringer, M. Mansfield, N. J. Mayne, T. Mikal-Evans, E. Palle, E. Schlawin, O. Shorttle, P. J. Wheatley, and S. N. Yurchenko, *Nature* **617**, 483–487 (2023).